Biogeochemical role of subsurface coherent eddies in the ocean: Tracer cannonballs, hypoxic storms, and microbial stewpots?

Ivy Frenger[1], Daniele Bianchi[2], Carolin Stührenberg[1], Andreas Oschlies[1,3], John Dunne[4], Curtis Deutsch[5], Eric Galbraith[6,7], Florian Schütte[1]

This article has been accepted for publication and undergone full peer review but has not been through the copyediting, typesetting, pagination and proofreading process, which may lead to differences between this version and the Version of Record. Please cite this article as doi: 10.1002/2017GB005743

Abstract. Subsurface coherent eddies are well-known features of ocean circulation, but the sparsity of observations prevents an assessment of their importance for biogeochemistry. Here, we use a global eddying (0.1°) ocean-biogeochemical model to carry out a census of subsurface coherent eddies originating from eastern boundary upwelling systems (EBUS), and quantify their biogeochemical effects as they propagate westward into the subtropical gyres. While most eddies exist for a few months, moving over distances of 100s of km, a small fraction (¡ 5 %) of long-lived eddies propagates over distances

Ivy Frenger & Daniele Bianchi, ifrenger@geomar.de & dbianchi@atmos.ucla.edu

[1]GEOMAR Helmholtz Centre for Ocean

Research Kiel, Kiel, Germany

[2]University of California, Los Angeles,

Los Angeles, USA

[3]Kiel University, Germany

[4]NOAA Geophysical Fluid Dynamics

Laboratory, Princeton, USA

[5]University of Washington, Seattle, USA

[6]Universitat Autonoma de Barcelona,

Barcelona, Spain

[7]ICREA, Barcelona, Spain

greater than 1000 km, carrying the oxygen-poor and nutrient-rich signature of EBUS into the gyre interiors. In the Pacific, transport by subsurface coherent eddies accounts for roughly 10 % of the offshore transport of oxygen and nutrients in pycnocline waters. This "leakage" of subsurface waters can be a significant fraction of the transport by nutrient-rich poleward undercurrents, and may contribute to the well-known reduction of productivity by eddies in EBUS. Furthermore, at the density layer of their cores, eddies decrease climatological oxygen locally by close to 10 %, thereby expanding oxygen minimum zones. Finally, eddies represent low-oxygen extreme events in otherwise oxygenated waters, increasing the area of hypoxic waters by several percent and producing dramatic short-term changes that may play an important ecological role. Capturing these non-local effects in global climate models, which typically include non-eddying oceans, would require dedicated parameterizations. **Keypoints:**

- We provide a model-based phenomenology of subsurface coherent eddies originating from eastern boundary upwelling systems.
- Eddies cause long-distance transport of biogeochemical tracers ("cannonballs"), contributing to the low-latitude mean state.
- Eddies represent low-oxygen extreme events ("hypoxic storms"), supporting low-oxygen processes outside oxygen minimum zones ("stewpots").

1. Introduction

A myriad of eddies at scales of $\mathcal{O}(10)$ to $\mathcal{O}(100)$ km has been recognized to populate the surface ocean at any time [*Chelton et al.*, 2011], showing up as beautiful swirls in high resolution satellite images such as ocean color and as sea surface height anomalies. In contrast, the occurrence and pathways of *interior ocean* eddies are much less well-known. Sporadic observations of interior ocean eddies, often labeled as "submesoscale coherent vortices" [*McWilliams*, 1985; *Riser and Owens*, 1985], have also been known for decades. They are often described as swirl-like currents associated with distinct lens-shaped tracer anomalies. These subsurface eddies reside within or below the pycnocline and are typically anticyclonic. They tend to be in geostrophic or gradient-wind balance and exist in the submesocale to mesoscale range [smaller and larger than the first baroclinic radius of deformation, *McWilliams*, 1985; *Collins et al.*, 2013; *Pelland et al.*, 2013; *Johnson and McTaggart*, 2010; *Molemaker et al.*, 2015]. The formation of subsurface coherent eddies may arise from baroclinic instabilities, just as for surface ocean eddies. However, subsurface eddies can also form from convection, or boundary currents undergoing flow separation, centrifugal and submesoscale instabilities that adjust into submesoscale or mesoscale balanced flows [*McWilliams*, 1985; *D'Asaro*, 1988; *Molemaker et al.*, 2015; *Gula et al.*, 2016; *Solodoch et al.*, 2016; *Bosse et al.*, 2016]. Their physical and biogeochemical tracer characteristics, from salinity to oxygen, indicate an origin in water masses foreign to the locations where the eddies are found [e.g., *Riser and Owens*, 1985; *Lukas and Santiago-Mandujano*, 2001]. These observations suggest that subsurface coherent eddies trap waters and transport them over vast distances in the relatively quiescent realm of the interior ocean. For

example "Meddies" were estimated to account for 40 % of the Mediterranean outflow and contribute to "a substantial part of the westward salinity flux in the Mediterranean water salt tongue" [*McWilliams*, 1985]. Similarly, subsurface "Cuddies" shedding from the California Undercurrent or "intra-thermocline-eddies" shedding from the Peru-Chile Undercurrent move anomalously salty, warm, oxygen-poor and nutrient-rich waters away from the coast [*Morales et al.*, 2012; *Collins et al.*, 2013; *Hormazabal*, 2013], well into the interior of the subtropical gyres [*Lukas and Santiago-Mandujano*, 2001]. Such non-local transport (labeled here *cannonball*-effect, see schematic in Figure 1) is not represented in typically non-eddying ocean and climate models because the coherent eddies' tracer anomalies are not related to local climatological density or tracer gradients [*Treguier et al.*, 2003].

For marine biogeochemistry, subsurface coherent eddies are not only interesting for their long-range tracer transports: the isolation of the eddies from surrounding waters provides a chemical environment distinct from the local climatological conditions and may directly affect biogeochemical and ecological processes within the eddies (Figure 1). Subsurface coherent eddies that originate from poleward-flowing undercurrents in EBUS, and subsequently propagate westward into the interior of subtropical gyres have caught much attention as rare, extreme low-oxygen events, which we refer to as *hypoxic storms* [e.g. *Lukas and Santiago-Mandujano*, 2001; *Johnson and McTaggart*, 2010; *Schütte et al.*, 2016b; *Stramma et al.*, 2013, 2014; *Karstensen et al.*, 2015]. The nearly anoxic conditions found in some of these eddies would limit the activity of oxygen-dependent heterotrophic organisms, and host a different microbial community than the surrounding oxygenated waters [*Löscher et al.*, 2015], potentially supporting anaerobic metabolisms, including denitrifi-

cation. We label the potential amplification of low-oxygen processes within eddies the *stewpot*-effect. Indeed, observations suggest that low-oxygen eddies can be hot-spots of fixed nitrogen losses [*Altabet et al.*, 2012; *Löscher et al.*, 2015] and production of nitrous oxide [*Arévalo-Martínez et al.*, 2016; *Grundle et al.*, 2017], a powerful greenhouse gas. Depending on their magnitude, the *cannonball*, *hypoxic storm*, and *stewpot* effects may require dedicated parameterizations in non eddy-resolving models. However, no global estimate of the importance of these effects exists so far.

In this paper, we focus on the prominent subsurface coherent eddies originating in the EBUS and propagating offshore. We label them "Puddies" due to their typical origin from the eastern boundary *p*oleward *u*ndercurrents. Because of the sporadic occurrence and extreme anomalies of Puddies, quantification of their large-scale influence requires data at high spatio-temporal resolution. Given that such a quantification cannot currently be carried out with the sparse existing network of subsurface biogeochemical observations, we instead use the output from a high-resolution global eddying model. Specifically, we (i) provide a phenomenology of subsurface coherent eddies originating from eastern boundary upwelling systems, and explore to what extent Puddies: (ii) account for a significant non-local biogeochemical tracer transport, moving oxygen-poor and nutrient-rich waters from EBUS to the subtropical gyres and thereby reshaping oxygen minimum zones (*cannon-ball*-effect); (iii) represent extreme low-oxygen events that may affect ecosystems (*hypoxic storms*) and (iv) contribute to the occurrence of denitrification and other anaerobic processes in otherwise oxygenated waters (*stewpot*-effect). To this end, we identify and track the eddies in the model, assess their properties and estimate their effect on biogeochemical tracer distributions and transports.

The rest of the paper is organized as follows: section 2 introduces the model and methods; section 3 details the results of the analysis; section 4 discusses the large-scale biogeochemical effect of Puddies; section 5 concludes the paper with implications for modeling and observational efforts.

2. Methods

2.1. Eddying Ocean Model

Because the observational record of subsurface coherent eddies is extremely limited in space and time, we focus on output from Geophysical Fluid Dynamics Laboratory (GFDL) CM2.6, a global coupled climate model with an eddying ocean. The model is characterized by: (i) a spatial resolution of 0.1°, thus actively-eddying [*Griffies et al.*, 2015], and resolving the mesoscale at low to mid latitudes in the open ocean [*Hallberg*, 2013], and (ii) a simple biogeochemical component (miniBLING), with three prognostic biogeochemical tracers including oxygen, and a single limiting macronutrient [*Galbraith et al.*, 2015]. Denitrification and nitrogen fixation is not represented in miniBLING, making the single macronutrient behaving akin to phosphate. miniBLING performs similarly to more sophisticated biogeochemical models in many respects [*Galbraith et al.*, 2015], making the model suitable to estimating the contribution of eddies to biogeochemical tracer budgets. The vertical resolution of the model comprises 50 levels with a spacing of 10 - 100 m at the depth range of 100 - 700 m where the eddies occur, largely sufficient to resolve subsurface eddies with vertical extents of several hundred meters. The model has been initialized from World Ocean Atlas 2009 [temperature, salinity, oxygen, phosphate: *Locarnini et al.*, 2010; *Antonov et al.*, 2010; *Garcia et al.*, 2010a, b] and Global Ocean Data Analysis Project [GLODAP, *Key et al.*, 2004], and run under preindustrial atmospheric carbon

dioxide concentrations for 200 years. miniBLING is coupled to the simulation after the initial spin-up of the physical model at year 48. For our analysis we use climatological and 5-day average fields from the last 20 years of the simulation to provide robust statistics of subsurface eddy numbers and properties.

The model physical and biogeochemical fields, and the ocean circulation, are largely spun up in the upper ocean over the last 20 years of the simulation, and have been shown to compare well to observations [*Griffies et al.*, 2015; *Dufour et al.*, 2015]. For the purpose of this study, we additionally carry out a brief evaluation of the climatological oxygen conditions, the representation of the eastern boundary poleward undercurrents, and the simulation of Puddies (see Results section 3.1).

2.2. Observational Data Used for Model Evaluation

We compare the model with four types of observational products: (i) a gridded global climatology, (ii) in-situ observations from moorings and gliders, (iii) shipboard acoustic Doppler current profile (sADCP) data, and (iv) observationally-based statistics of North Atlantic subsurface coherent eddies. In detail, the corresponding observations we used are (i) physical and biogeochemical fields of the climatology CARS 2009 from http://www.marine.csiro.au/ dunn/cars2009 [*Condie and Dunn*, 2006] which incorporates data of the past 50 years; (ii) physical and biogeochemical mooring data available at http://uop.whoi.edu/currentprojects/Stratus/stratus.html as detailed in *Stramma et al.* [2014]; (iii) South Pacific poleward undercurrent data collected by IMARPE (Peruvian Institute of the Sea) and used as in *Chaigneau et al.* [2013], and North Pacific undercurrent data collected by the CUGN [California Underwater Glider Network, *Rudnick et al.*,

2017], available at http://spraydata.ucsd.edu/climCUGN; and (iv) eddy statistics from *Schütte et al.* [2016a, b].

2.3. Detection of Puddies

To assess the characteristics and effects of Puddies, we take the approach of identifying individual eddies in the model and tracking them over time in an automated manner to have a large sample size available for subsequent analysis [based on *Faghmous et al.*, 2015]. Typically, mesoscale eddies are identified from their sea surface height anomaly signatures. As a sea surface height anomaly is anticipated to be weak or missing for subsurface ocean eddies, a detection is required in the ocean *interior*. To this end, we determine representative density surfaces embracing Puddies and identify eddies as positive anomalies of the layer thickness bounded by these densities. We then follow the identified eddies from one time step to the next, i.e. we track them over time. We discuss each of these steps in the following sections.

2.3.1. Determining the Relevant Density Layers

We focus on four regions that extend westward from the main EBUS in the Atlantic and Pacific basins, shown as black boxes in Figure 2a. Snapshots of individual Puddies provide an impression of the density range in which the eddies reside (Figures 2c,3a). This range is systematically assessed as follow. First, we set the meridional range of the focus regions based on low oxygen conditions at the depth/density of the eddies, and the existence of a poleward undercurrent from which the eddies are thought to originate (see Figures 4a,5a). Second, we pick inshore and further offshore meridional sections of the Okubo-Weiss parameter across these regions [*Okubo*, 1970; *Weiss*, 1991, see e.g. for the

South Pacific, the white dashed line in Figure 2a].

A negative Okubo-Weiss parameter represents a dominance of vorticity (i.e. rotation) over strain, hence indicating the presence of a vortex, or eddy. Because eddies are transient, showing up as temporal negative anomalies of the Okubo-Weiss parameter, we set positive values of the Okubo-Weiss parameter to zero to discard dominance of strain, and next calculate the temporal standard deviation of the Okubo-Weiss parameter over 20 years of 5-daily data. The depth-range of subsurface eddies appears as a maximum of the standard deviation below the mixed layer depth, and below the maximum vertical gradient of the pycnocline (Figure 3b).

Based on this analysis, we pick σ=26.4 kg m^{-3} and σ=27.1 kg m^{-3} as upper and lower bounding densities, corresponding to densities which embrace high standard deviations of the Okubo-Weiss parameter. This range is fairly representative for both the Pacific and Atlantic basins. Our conclusions are not particularly sensitive to choosing slightly lighter or heavier density layers, as long as they correspond to the circa 100 m - 700 m depth range at which the Puddies' cores are found (Figures 2c,3a).

Anticyclonic subsurface eddies are lens-shaped, with upward doming isopycnals above the eddy core, and depressed isopycnals below it (Figure 2b,c). For cyclonic eddies, the opposite is true, i.e. isopycnals are depressed above the eddy core, and domed below it. Density surfaces bounding the eddies are similar close to the coast and further offshore. This indicates that Puddies tend to conserve their density, that is, they slide along isopycnals as they subduct from the formation regions into the gyre interiors.

After extracting the thickness of the density layer between 26.4 kg m^{-3} and 27.1 kg m^{-3},

we calculate 5-day anomalies relative to the climatological thickness, and finally identify eddies based on positive thickness anomalies (see Methods section 2.3.2 below). As indicated in section 1 we focus on thick (positive) anomalies, i.e. low-stratification lens-shaped anticyclonic Puddies, leaving aside highly-stratified cyclones. This choice is motivated by the fact that, even though subsurface cyclonic eddies have been observed (e.g. south of Australia in *Frenger et al.* 2015), the lens-shaped anticyclonic eddies have been prevalent in observations for decades. The apparent dominance of weakly-stratified eddies in both observations and models [*Kurian et al.*, 2011; *Nagai et al.*, 2015] is consistent with the formation of Puddies by subsurface boundary currents through flow separation, which is expected to favor the generation of low potential vorticity waters, i.e. anticyclones [*McWilliams*, 1985; *D'Asaro*, 1988; *Dewar et al.*, 2015; *Molemaker et al.*, 2015; *Thomsen*, 2016].

2.3.2. Identification and Tracking

We identify Puddies from closed contours of positive isopycnal layer thickness anomalies (see previous section 2.3.1) using the method of *Faghmous et al.* [2015, associated code available at http://dx.doi.org/10.5281/zenodo.13037], which was originally developed to detect mesoscale eddies from their sea level height anomalies. The identification algorithm first searches for local extrema of the input field, e.g. maxima, which are identified as the centers of anticyclones. Once an extremum is found, the algorithm reduces the value found at the center by an incremental step, and determines an associated closed contour around the center. If the closed contour still contains only a single maximum, the contour value will be iteratively decreased, followed by the check that the contour still contains a single maximum. Once the contour encloses more than one single maximum,

the algorithm stops and the closed contour from the preceding step is used as definition of the eddy boundary. This method does not require specification of a maximum eddy size as typically done for closed-contour approaches [e.g., *Chelton et al.*, 2011]. In short, Puddies are defined as the largest (outermost) closed contours of layer thickness anomalies containing only a single maximum.

We chose the following input parameters for the algorithm: the incremental increase is set to 0.05 m and the minimum area of eddies to 4×4 (i.e. 16) pixels to resolve the eddy radius with at least two grid boxes. Two grid boxes correspond to roughly 20 km or about half of the first baroclinic radius of deformation, with the latter representing a rough expectation of the eddy length scale [*McWilliams*, 1985; *Kurian et al.*, 2011]. Hence, the resolution of the model is expected to be sufficiently high to resolve mesoscale Puddies. Note that formation of Puddies in finer resolution models involves submesoscale adjustment processes after the detachment of the undercurrent from the shelf, and upscale organization into geostrophic or gradient wind balanced currents [*Molemaker et al.*, 2015]. In the mesoscale-resolving model used for the present study, Puddies presumably form directly from boundary current instabilities as balanced flow [*Hormazabal*, 2013; *Combes et al.*, 2015; *Molemaker et al.*, 2015; *Solodoch et al.*, 2016].

We track the closed contours, i.e. Puddies over time with a modified version of the nearest-neighbor-approach provided by *Faghmous et al.* [2015] where the search space for an eddy in each subsequent time is based simply on the eddy radius: following detection on one time step, we search for the eddy in the next time step, i.e. five days later, within a circle surrounding the presumed location of the eddy center, estimated based on the propagation of the previous time step. The radius of the circle is set to the radius of the

eddy with a cap at 60 km. The eddy is allowed to disappear for up to 20 days to bridge time periods during which the eddy is lost to the identification algorithm and thus to prevent a premature cut of an eddy-track: an eddy may be lost for consecutive time steps if it is characterized by multiple extrema. Multiple extrema within a large eddy are identified by the algorithm as individual features which are discarded if they are too small to pass the 4×4-threshold size. Within 20 days the average eddy propagates over a distance corresponding roughly to its radius (see Results section 3.2), so that if an eddy is lost and another eddy detected inside the radius within the following 20 days, it is very likely the same eddy at a later time. The identification and tracking of eddies was evaluated visually based on animations (see sample animations in the Supplementary Material). The choice of algorithm parameters is conservative, in the sense that we prefer to end an eddy-track prematurely, rather than merge tracks of independent eddies. Based on sensitivity tests (not shown), we do not expect our conclusions to be sensitive to the exact choice of the parameters of the identification and tracking algorithms.

Following identification and tracking, we quantify the following eddy properties: the radius L_e, defined as the radius of a circle with an area equal to the eddy area; the eddy lifespan, defined as the time period between the first and the last identification of an eddy; and the lifetime propagation distance.

As our focus is on subsurface coherent eddies that originate from EBUS and carry their typical chemical signature into the gyres, i.e. Puddies, we filter tracked eddies according to the following criteria: we constrain our analysis to eddies that (i) originate in climatological oxygen conditions of 200 μmol kg^{-1} or less, and that (ii) feature a net westward propagation over their lifetime. Many of the closed-contour features detected as eddies

are quite short-lived i.e. with lifespans of few weeks. To ensure a certain coherence and lifetime propagation distance, we further consider eddies only if they exist for at least 3 months; for the assessment of long-range transport, we limit our analysis to eddies existing at least 9 months. Finally, we consider only eddies with complete life cycles, i.e. we discard eddies existing in the first or last time step of the analysis period, and further discard the first and last 2 years of the 20 year simulation time to ensure a full lifespan spectrum during the analysis period.

We note that we refer to *coherent* eddies as (i) vortex-like structures (ii) associated with density anomalies, (iii) which remain coherent and conserve material properties as they propagate over distances larger than their size. From (iii) it follows that tracer properties of coherent eddies are generally different from ambient waters, an indicator for their distant origins. The dilution of tracers over the eddies' lifetime provides a measure for the entrainment of external waters, i.e. a measure of the imperfect coherence of the eddies (see the Results sections 3.4.1/4.1). With respect to coherency, our definition is not as strict as the definition of eddies as *Lagrangian coherent structures* [see e.g. review by *Haller*, 2015], which by design are expected to preserve 100 % of the water in their core.

2.3.3. Collocation of Puddies and Tracer Properties

To determine the Puddies' tracer characteristics we proceed as follows. (i) We interpolate the 5-day biogeochemical (oxygen and macronutrient) and physical (temperature and salinity) fields on an isopycnal layer roughly at the cores of the eddies, here 26.7 $\mathrm{kg\,m^{-3}}$ (Figures 2c,3a). (ii) We apply a low-pass filter, i.e. smooth the resulting fields by convolution with a 10×10 box kernel, roughly corresponding to the mean eddy diameter. This rather large filter provides a conservative estimate: if a smaller or no filter is chosen, eddy

effects are qualitatively similar, yet larger as eddy properties are more extreme at the eddy core. (iii) We extract from these fields (unsmoothed and smoothed) the values at the center of each eddy. Thereby, we take the unsmoothed fields to represent extremes associated with eddies, and the smoothed fields to be representative of the eddies' cores. Estimates of sea surface height anomalies associated with subsurface eddies are calculated conservatively as the difference between 5-day mean sea surface height fields smoothed with 10×10 box and 30×30 box filters. We also extract tracer values and remineralization rates at eddy centers from climatologies, as due to data storage constraints, remineralization rates were not stored at sufficiently high resolution to directly diagnose effects of Puddies. Climatologies are calculated as averages over the last 20 years of the model simulation, i.e. years 181 - 200, and tracer anomalies are then calculated relative to the climatologies.

2.4. Biogeochemical Effects of Puddies: Transport and Sources-Sinks

2.4.1. Long-Range Volume and Tracer Transports

We estimate the volume export by Puddies from a region, such as the inshore regions shown in Figure 2a with the following equation [see also *McWilliams*, 1985]:

$$M_{\mathrm{e}} = n_{\mathrm{e}} V_{\mathrm{e}} [\mathrm{m}^3\,\mathrm{s}^{-1}]\,, \tag{1}$$

where n_{e} is the average number of eddies leaving each region per unit time ($[\mathrm{s}^{-1}]$). The average eddy volume $V_{\mathrm{e}} = \frac{4}{3}\pi L_{\mathrm{e}}^2 \frac{1}{2}\mathrm{H}_{\mathrm{e}}$ ($[\mathrm{m}^3]$) is approximated as a spheroid, with the eddy thickness H_{e}=100 m, a lower bound estimate (see also Figure 2c), and L_{e} the eddy regional average radius.

The component of the tracer convergence due to long-range transport by Puddies in the

same regions per unit mass is estimated with:

$$\Delta D_{\mathrm{e}} = \rho_0 \, \Delta C_{\mathrm{e}} \, M_{\mathrm{e}} \, M^{-1} \, \mathrm{T} \, [\mu\mathrm{mol\,kg^{-1}\,yr^{-1}}] \,, \tag{2a}$$

$$D_{\mathrm{e}} = \rho_0 \, C_{\mathrm{e}} \, M_{\mathrm{e}} \, M^{-1} \, \mathrm{T} \, [\mu\mathrm{mol\,kg^{-1}\,yr^{-1}}] \,, \tag{2}$$

with ρ_0 denoting a reference density ($1035\,\mathrm{kg\,m^{-3}}$), ΔC_{e} the regional average tracer concentration anomaly of eddies ($[\mu\mathrm{mol\,kg^{-1}}]$), the volume of the region M ($[\mathrm{m^3}]$) and T converting from seconds to years. In addition to the eddy average anomalous tracer concentration ΔC_{e} in equation (2a), we also use the average eddy tracer concentration C_{e} to estimate the tracer convergence due to the eddies' water volume transport in equation (2). ΔD_{e} based on equation (2a) and D_{e} based on equation (2) can then be compared to the terms of the tracer tendency [see e.g., *Griffies et al.*, 2015, 2016] calculated online. The tracer tendency is largely determined by a balance between the convergence of resolved advective processes (D) and the tracer sources/sinks, while the convergence of parameterized subgridscale advective and diffusive processes is small (except for the inshore Atlantic region where vertical diffusion of the macronutrient is similar to sources-sinks, not shown). The tracer concentration C and the resolved flow $\mathbf{v}$ (multiplied by the conversion factor T and normalized by M to obtain $[\mu\mathrm{mol\,kg^{-1}yr^{-1}}]$) were uset to calculate $D = -\nabla \cdot (\rho_0 \mathbf{v} C)$ online (i.e. during the simulation). The result encompasses both the convergence of the long-range subsurface coherent eddy transport D_{e}, which is estimated separately based on equation (2) and non-coherent contributions. To gauge the relative importance of the coherent transport, we directly compare the two terms.

To illustrate some of the uncertainty of the estimates of tracer transport by Puddies based on equations (2a,2), we add error bars to the budget figures in Results section 3.4.2, based on the standard error of the radii and eddy numbers, and increasing their thickness from

100 m to 200 m.

For the comparison of D_e and D we consider an inshore EBUS volume, as noted above, and an offshore subtropical gyre volume. The lateral boundaries of these regions, shown in Figures 2a and 9c, are defined as ranging from the coast to 500 km offshore (inshore, EBUS), and from 500 - 4000 km offshore (offshore, subtropical gyre). The vertical extent of the volumes is the same isopycnal layer chosen for the eddy detection (26.4 kg m^{-3} and 27.1 kg m^{-3}, Figure 3b), hereafter referred to as the pycnocline.

2.4.2. Contribution to the Mean State

Puddies moving away from EBUS regions typically carry with them a low-oxygen signature. Therefore, their presence modifies the climatological shape and intensity of oxygen minimum zones, presumably diminishing their intensity and expanding them towards the well-oxygenated subtropical gyres. The contribution of Puddies to the mean tracer (i.e. oxygen) concentration can be estimated based on [see also *Schütte et al.*, 2016b]:

$$C = f_e \cdot C_e + (1 - f_e) \cdot C_{ne} \tag{3}$$

Where C is the climatological (i.e. long-term time mean) tracer concentration, which already includes the eddy contribution, C_e as in equation (2) is the average tracer concentration inside the eddies, and f_e is the probability a transient Puddy is present at a given location, which we refer to as eddy coverage. The unknown is C_{ne} which represents an estimate of the tracer field if the eddies were not present. Solving equation (3) for this term results in

$$C_{ne} = (C - f_e \cdot C_e) \cdot (1 - f_e)^{-1} \tag{4}$$

where all the terms on the right hand side can be calculated based on model output and the subsequent eddy tracking results. After obtaining C_{ne} with this approach, we compare

it to the actual climatological tracer C to assess to what extent Puddies alter the mean state tracer distribution.

3. Results

3.1. Model evaluation

3.1.1. Mean State Relevant to the Simulation of Puddies

The depth of the ocean isopycnal layer on which Puddies typically reside (26.7 $\mathrm{kg\,m^{-3}}$, see Methods section 2.3.3), as well as the pattern of dissolved oxygen in this layer, compare favorably with observations, showing the typical transition from deeper oxygenated subtropical waters to shallower, low-oxygen tropical and EBUS waters (Figure 4a,b). The difference between model and observations (CARS, see Methods section 2.2) tends to show overestimated oxygen concentrations, most pronounced in the Southeast Pacific, with the exception of low inshore oxygen concentrations in the tropical Atlantic (Figure 4c). These biases largely covary with the biases in the density structure: where the isopycnal is shallower than observations, oxygen concentrations tend to be higher. The oxygen overestimate in the South Pacific may arise from a bias toward deep winter mixed layers in the Southeast Pacific sector of the Southern Ocean (not shown), injecting abundant well-oxygenated waters onto this isopycnal surface. Part of the bias may also be due to an overly strong ventilation by the zonal southern Tsuchiya Jet in the model. A high bias of oxygen concentrations in coastal regions, where Puddies originate, may cause an initial high oxygen bias in Puddies. The offshore oxygen gradient in the Pacific largely agrees with that observed, but in the Atlantic, the oxygen gradient is exaggerated by the model. This suggests that estimates of long-range transport by Puddies in the Atlantic should be

taken with additional caution.

Because Puddies tend to be shed from EBUS poleward undercurrents, the model should reasonably represents these currents, in order to accurately capture the eddies' biogeochemical impact. While a comprehensive characterization of EBUS undercurrents is beyond the scope of this study, a preliminary analysis shows that undercurrents exist in the model (Figure 5a) and resemble in-situ observations in the North and South Pacific (Figure 5b). Note that the along-shore and temporal variability of poleward undercurrents is large [see e.g., *Chaigneau et al.*, 2013; *Rudnick et al.*, 2017, and Figure 5a] and not well characterized. Hence, it is difficult to assess the representativity of available observations. Nonetheless, overall, undercurrents appear to be wider and weaker in the model than in the real ocean, potentially leading to an underestimate of the eddy generation rates and intensities [*Molemaker et al.*, 2015; *Thomsen*, 2016].

3.1.2. Qualitative Representation of Puddies

The model simulates abundant Puddies with anomalous low-oxygen signatures (Figure 2a,b). An exhaustive comparison of model subsurface coherent eddies with observations is not possible, given the small number of available observations. However, comparison of an observed Puddy from the South Pacific with a simulated Puddy in the same location shows similar features (Figure 2c), including a distinct low oxygen extreme in the pycnocline, and the typical lens-shape.

The comparison of the individual South Pacific Puddy hints that oxygen concentrations of model Puddies are biased high (Figure 2c,d), as does a comparison of the average oxygen concentration of North Atlantic Puddies ($66\,\mu\mathrm{mol\,kg^{-1}}$, *Schütte et al.*, 2016b, vs.

124 μmol kg^{-1} for model eddies). Further, Puddies with next to anoxic conditions are exceptional in the model (2 % have concentrations below 5 μmol kg^{-1}), while they appear to be common in observations [*Lukas and Santiago-Mandujano*, 2001; *Schütte et al.*, 2016b; *Stramma et al.*, 2014]. The magnitude of oxygen anomalies in the model and observations can be similar for individual Puddies (e.g. the South Pacific eddy in Figure 2d). However, for the majority of Puddies anomalies are too weak, at least in selected regions (*Schütte et al.*, 2016b, find average anomalies of -100 μmol kg^{-1} of North Atlantic Puddies, contrasting with much smaller average anomalies close to -10 μmol kg^{-1} in the model).

The partial mismatch of oxygen concentrations and anomalies may be due to (i) the tendency of a high oxygen bias in the model where Puddies form, at least in the Pacific (Results section 3.1.1, see also white contours in Figure 5b), (ii) underrepresented or missing biophysical interactions associated with Puddies in the model. Biophysical interactions have been observed to lead to an apparent oxygen utilization rate within Puddies that is several times to an order of magnitude larger compared to surrounding waters [e.g., *Stramma et al.*, 2013; *Karstensen et al.*, 2015; *Schütte et al.*, 2016b], possibly caused by feedbacks of the eddy on surface productivity and export, or increased transport and remineralization of organic matter within the eddies. Finally, (iii) a sampling bias in observations may also contribute, whereby intense, low-oxygen eddies are preferentially detected or described.

The locations and pathways of Puddies visually agree well with observations in the South Pacific and North Atlantic oceans [see *Johnson and McTaggart*, 2010; *Schütte et al.*, 2016b, and Figure 6], with origins in EBUS and a subsequent offshore propagation. Quantitatively, we found 2 to 3 times as many eddies existing 3 months or longer in the North

Atlantic as compared to *Schütte et al.* [2016a]. The comparison to *Schütte et al.* [2016a] should be viewed with caution, however, as different eddy identification methods were used and the smaller number of observed eddies may be due to the restriction of observational studies to Puddies characterized by surface signals.

Puddies in both the model and observations tend to carry the temperature and salinity signature of the poleward eastern boundary undercurrents at similar latitudes (see snapshots of sample eddies, Figure 3a). That is, on average they are warmer and saltier than surrounding waters [e.g., *Lukas and Santiago-Mandujano*, 2001; *Stramma et al.*, 2014, Figure 7], except for the North Atlantic where they are fresher and cooler [*Karstensen et al.*, 2015; *Schütte et al.*, 2016a, Figure 7]. 76 % and 91 % of eddies existing at least 3 and 9 months, respectively, feature physical and biogeochemical characteristics of undercurrent waters. These numbers support the hypothesis that the majority of detected eddies originate from poleward undercurrents.

We conclude that the model simulates subsurface eddies sufficiently well to use its solution to provide a first global census of Puddies and a first estimate of their importance for biogeochemistry.

3.2. Statistics of Puddies

We focus on subsurface coherent eddies that are anticyclonic, exist 3 months or longer, form in EBUS waters with climatological oxygen levels smaller than 200 μmol kg^{-1}, and dissipate further offshore, i.e. feature a net westward propagation (see Methods section 2.3.2). This subsampling, mainly due to the constraint on age, drastically reduces the number of eddies, leaving us with a few percent of the initially tracked features, or a total of 9101 (569/yr) eddies which are captured by more than 300,000 5 day-average snap-

shots. Of this subselection of eddies, 25 % (total 2250, 141/yr) exist 6 months or more, 9 % (total 812, 51/yr) 9 months or more, and 4 % (total 399, 25/yr) 12 months or more. We identified most eddies in the North Pacific, followed by the South Pacific, the South Atlantic and the North Atlantic.

There is significant interannual variability in eddy formation rates (not shown), and a weak seasonality, with a subtle peak of eddy formation in the Pacific in autumn. The latter contrasts with results by *Schütte et al.* [2016a] who noted a formation peak in the North Atlantic in spring. We anticipate variability of Puddy formation to be linked to poleward undercurrent variability, which in turn may be linked to both seasonal and interannual wind stress curl variations and large-scale climate modes. Seasonality and interannual variability of poleward undercurrents is not well known given the sparsity and sampling bias of observations [see e.g., *Chaigneau et al.*, 2013]. We leave variability of Puddy formation and its relation to poleward undercurrent variability for future work. While research exists on Puddy formation from poleward undercurrents [see Introduction, and e.g., *Molemaker et al.*, 2015; *Thomsen*, 2016], mechanisms of Puddy decay are less clear. As noted before, Puddies tend to form along a narrow coastal strip associated with poleward undercurrents, and to decay offshore, over a much wider region. Based on the sample animations in the Supplementary Material we identify a few qualitative aspects of eddy decay: (i) Puddies merge and split not only in coastal but also offshore waters, resulting in Puddy "deaths". (ii) Puddies strongly interact with islands and seamounts, resulting in Puddy splitting or dissipation (see sample animations in the Supplementary Material, especially associated with the Hawaiian islands and the ridge east of Easter Island, in the North and South Pacific basins, respectively). Accordingly, Puddy coverage

decreases downstream of such features (Figure 9a). (iii) Puddies in the open ocean become steadily smaller and/or unstable late in their lifetimes, shed filaments and subsequently dissolve, perhaps as a result of interaction with the background flow [*McWilliams*, 1985]. Distributions of eddy characteristics and their averages (10th percentiles/90th percentiles) are given in Figure 7a-d and Table 1, and their physical and biogeochemical anomaly extrema (see Methods section 2.3.3) in Figures 7e,8a-d and in Table 2. Note that the distributions of eddy characteristics are skewed towards small mean values with long tails of extrema, especially for biogeochemical tracers. Compared to observational estimates based on Argo profiling floats, these anomalies are of the same sign, yet clearly smaller [*Schütte et al.*, 2016a; *Pegliasco*, 2015]. Causes for the smaller magnitude of anomalies in the model include: (i) potential model biases; (ii) a focus of observational studies on pronounced eddies, such as on eddies with a large radius and/or sea surface height anomaly; and (iii) the limitation to subsurface eddies with a detectable surface signal, which would favor subsurface eddies which are intense.

We also tracked cyclonic subsurface eddies. The results suggest that anticyclones dominate in the pycnocline, accounting for 60 % and 80 % of all of 3 month and 9 month-lifespan subsurface coherent eddies, respectively. Furthermore, outside of the North Atlantic, cyclonic eddies do not tend to carry the low-oxygen, high-macronutrient or temperature/salinity characteristics of poleward undercurrents. Because of their very different characteristics, we leave an investigation of subsurface cyclonic eddies for future studies.

Puddies feature a positive sea surface height anomaly for 60 % and around 75 % of the eddies existing 3 months and 9 months or longer, respectively (Figure 7f). The average anomaly is subtle: 1.2 cm for 9 month eddies and even smaller for 3 month eddies. This

is smaller than the several centimeters diagnosed by [*Stramma et al.*, 2014; *Schütte et al.*, 2016b]. Note that the latter study detected eddies based on their surface signal, i.e. missing eddies with a weak surface expression. Hence their estimate of the sea surface height anomaly is anticipated to be biased high. We find an indication that the surface signature weakens for Puddies that "hide" in the pycnocline below 300 - 400 m depth. Our results corroborate earlier studies that surface-based detection of subsurface coherent eddies may prove challenging [see also *Bashmachnikov*, 2014; *Assassi et al.*, 2016; *Ciani*, 2017]. For instance, an index based on a combination of sea surface height and sea surface temperature [*Schütte et al.*, 2016a; *Assassi et al.*, 2016] to distinguish surface intensified and subsurface intensified eddies, will fail if sea surface height anomalies are negative, as is the case for a non-negligible fraction of subsurface eddies in the model (Figure 7f).

The coverage of Puddies (f_e, see Methods section 2.4.2) existing at least 3 months can exceed 10 % in the areas adjacent to EBUS (Figure 9a). It is largest inshore and tends to level off further offshore. This is anticipated if most eddies are formed near the coast from poleward undercurrents. Note that not all eddies form directly near the coast. Eddies appearing further offshore may result from difficulties in tracking, or from offshore formation by merging of filaments or splitting of existing eddies (see sample animations in the Supplementary Material).

3.3. Potential Effect of Puddies on Biogeochemical Sources-Sinks

3.3.1. Contribution to Climatological Biogeochemical Tracer Field

Average biogeochemical tracer anomalies representative over cores of Puddies (see Methods section 2.3.3) existing 3 months or longer are in the range of -4 to -14 μmol kg^{-1} for oxygen and close to 0.1 μmol kg^{-1} for the macronutrient in the four regions. These anoma-

lies are larger for long-lived eddies existing 9 months or longer, namely in the range of -8 to -39 μmol kg^{-1} for oxygen and 0.1 to 0.2 μmol kg^{-1} for the macronutrient.

As a result, the contribution of Puddies to the climatological oxygen field is to decrease oxygen levels by a few percent and up to 10 % (Figure 9c), supporting the results by *Schütte et al.* [2016b] who found a similar decrease of roughly 10 % due to eddies in the North Atlantic shallow oxygen minimum. A significant effect of eddies on climatological oxygen occurs where eddies are numerous (Figure 9a) and where the oxygen tracer gradient along their propagation path is steep (see contours in Figure 9b,c), i.e. their anomalies are large (Figure 9b). The oxygen decrease due to eddies results in a subtle westward expansion of the large-scale oxygen-minima (black solid versus dashed contours in Figure 9c). Hence, to some extent, Puddies contribute to shaping the mean biogeochemical state of the pycnocline.

3.3.2. Contribution to Biogeochemical Extreme Events

Puddies represent low-oxygen extreme events at the locations where they occur (Figure 10). The transient low-oxygen-Puddy lenses may affect the behavior of motile oxygen-sensitive organisms in the ocean, e.g. vertically migrating zooplankton and larger predators [*Bianchi et al.*, 2013; *Stramma et al.*, 2011; *Hauss et al.*, 2016], place stress on benthic communities where they impinge on the seafloor, or allow for suboxic biogeochemical processes, such as reduced particle degradation, increased nitrous oxide production and denitrification [*Löscher et al.*, 2015]. These processes are typically focused inside oxygen minimum zones, but in association with eddies, they may happen outside the climatological boundary of oxygen minimum zones. For example, on the isopycnal layer 26.7 kg m^{-3}, at climatological oxygen concentrations >30 μmol kg^{-1} (i.e. outside of climatologically

suboxic waters), the average total volume of suboxic Puddies is equal to 5 % of the global suboxic water volume. Similarly, at climatological oxygen concentrations >90 μmol kg^{-1} (i.e. outside of climatologically hypoxic waters), the average total volume of hypoxic Puddies is equal to 10 % of the global volume of hypoxic waters.

While transient low-oxygen extreme events typically occur at the fringes of climatological oxygen minimum zones associated with instantaneous deformations of the oxygen minimum zone boundary, the low-oxygen extreme events associated with Puddies frequently occur far from this boundary in well-oxygenated waters of the subtropical gyres.

3.4. Long-Range Tracer Transport by Puddies

3.4.1. Coherence

Puddies tend to preserve material properties of their source waters. For instance, oxygen tends to hover around the same value over the lifespan of the average Puddy, especially in the Pacific (Figure 11a,c). The stable oxygen concentrations in simulated Puddies contrast with the ambient climatological oxygen concentrations, which increase as Puddies propagate westward into the subtropical gyre. In the Atlantic, this contrast is less pronounced, as oxygen inside the eddies increases with their lifetime, apparently because they are less coherent (Figure 11b,d, see also Figure 8). Accordingly, oxygen anomalies are smaller than in the Pacific, where oxygen concentrations remain closer to their initial values. That is, the evolution of oxygen concentrations in Pacific Puddies suggests a greater efficiency in isolating waters in their core than their Atlantic counterparts.

The oxygen concentrations within Puddies result from a balance between consumption in the eddy interior and physical supply across the eddy boundary. An estimate of the oxygen decrease due to cumulative oxygen consumption within eddies after their

formation (based on local climatological rates, see Methods section 2.3.3) indicates that the internal consumption is indeed a significant, but relatively minor effect in the Pacific (pink lines, Figure 11). The effect in the Atlantic is larger, presumably because Puddies are shallower and therefore experience higher rates of both remineralization and boundary exchange (see Figure 4). We conclude that, globally, lateral transport of low initial oxygen concentrations across large background gradients is the main cause of Puddy oxygen anomalies, though local consumption can make an important contribution, particularly in the Atlantic.

3.4.2. Biogeochemical Tracer Budget

Puddies will release their material properties where they dissolve further offshore, 100s to 1000s km away from the location where they enclosed water and material properties. Most (about 80 %) of the distance covered by Puddies over their lifetime is due to their intrinsic propagation rather than advection by the mean flow. This estimate is based on the westward zonal propagation speed of eddies relative to the climatological (i.e. ambient) westward flow averaged over 50 - 500 m depth (not shown). In the following, we estimate the Puddies' contribution to the biogeochemical tracer convergence, for both inshore EBUS and offshore subtropical gyre regions (as marked in Figures 2a,9c, see Methods section 2.4.1).

To this end, we compare the tracer convergence arising from the Puddies' transport to the tracer convergence due to all resolved advective processes, which encompass the Puddy transport (see Methods section 2.4.1). We focus on the contribution from long-lived Puddies existing 9 months or longer which propagate over long distances. We first discuss how the tracer convergence in the regions is altered by Puddies carrying a tracer anomaly

(equation (2a)), and second their absolute contribution to the tracer convergence (equation (2)).

First, Puddies affect total tracer advection because they carry biogeochemical tracer anomalies: for oxygen, they cause an *export* of anomalously *low*-oxygen waters from the inshore regions, driving a *positive* anomaly of the inshore oxygen convergence (Figure 12c), implicitly supporting oxygenation of the inshore regions. In contrast, in the offshore regions, Puddies *import* anomalously *low*-oxygen waters, leading to a reduced convergence of oxygen from advection. The onshore increase is around 10 % and the offshore reduction around 5 % in the Pacific, whereas the numbers are small for the Atlantic. The same holds for macronutrients, with the difference that the sign is flipped since Puddies carry high-macronutrient anomalies (Figure 12d). Therefore, because of their enhanced nutrient content relative to surrounding waters, Puddies act to extract nutrients from the coastal regions to redeposit them further offshore.

Second, we quantify the absolute magnitude of the long-range transport by Puddies. Below the surface, the net resolved flow supplies oxygen and removes macronutrients both in inshore and offshore waters (Figure 12a,b), thereby compensating for remineralization of organic matter, which depletes oxygen and releases macronutrients everywhere. Puddies form in the inshore regions and dissolve in the offshore regions. As part of this offshore volume transport, they also extract biogeochemical tracers, i.e. both oxygen and macronutrients from the EBUS and supply them to the offshore subtropical gyre. This Puddy-driven subsurface transport contributes $\mathcal{O}(10)$% to more than 100 % to the total advective tracer convergence in the Pacific pycnocline (Figure 12e,f). One needs to keep

in mind that this transport is associated with a compensating volume flow while the Puddies move westward. If the convergence due to Puddies is larger than the convergence of all resolved advective processes (i.e. if it is larger than 100 %), other advective processes, including undercurrent transport and eastward stretching filaments, are compensating for the Puddy-induced export of tracer from the region.

The results show a much smaller contribution of eddies to the total advective convergence in the Atlantic relative to the Pacific. The greater role of Puddies in the Pacific is due to both their larger numbers, and to weaker contributions from other advection terms in the region (Figure 12a,b). Further, there are tracer differences, with eddy oxygen transport in the Pacific ranging from around 10 % to more than 70 %, and macronutrient transport ranging from 30 % to around 150 % of the total transport. The muted and boosted contributions of Puddies to oxygen and macronutrient convergence, respectively, is consistent with Puddies carrying negative anomalies for oxygen and positive anomalies for macronutrients.

3.4.3. Indirect Ventilating Effect

To estimate the Puddies' effect on ventilation time scales in the inshore and offshore regions, we estimate their volume transport with equation (1). For volume, it does not matter where waters originate from, i.e. if it is long-range transport or not, therefore we relax our constraint on lifespan from 9 to 3 months. Then, the volume transport across the inshore-offshore boundary adds up to 0.1 Sv and 0.2 Sv for the North and South Atlantic, respectively, and 0.5 Sv for the Pacific Puddies. This is of the same order of magnitude as estimated by *Schütte et al.* [2016b] based on observations.

In comparison to the average poleward volume transport by the boundary undercurrents in the pycnocline, the volume export by Puddies existing 3 months or longer accounts for 10 % (North Atlantic), 30 % (South Atlantic, South Pacific) to close to 50 % (North Pacific) of the respective undercurrent transports. Thus, the model suggests that Puddies leak a substantial fraction of the low-oxygen, nutrient-rich undercurrent waters offshore. According to visual assessment (based on animations), export of these waters by Puddies is accompanied by high-oxygen, low-nutrient filaments intruding eastward, presumably supported by mass conservation as Puddies propagate westward, and/or by stirring of Puddies along isopycnals. The ventilation time scale of the pycnocline in the focus regions, due only to the export by Puddies and assuming a compensating influx of oxygenated waters, would then be $\mathcal{O}(10)$ years for all basins, except for the North Atlantic where it exceeds 200 years.

4. Discussion

4.1. Subsurface Coherent Eddies as Tracer *Cannonballs*

Observations have shown that tracer characteristics of Puddies do not evolve much over time [*Pegliasco*, 2015], suggesting that Puddies transport relatively isolated waters. Similarly, in the model we find Puddies to be coherent, in the sense that they trap water and tracers and carry them westward with their intrinsic propagation velocity (see Methods section 2.3.2 and Results section 3.4.1). Although the eddy boundaries are not impermeable to water exchange (we estimate a dilution of eddy core waters between 10 % in the Pacific to 80 % in the Atlantic, see Results section 3.4.1), there is a resulting long-range, i.e non-local, lateral transport that is not considered in the typically non-eddying ocean and climate models. Our results suggest this effect ranges from a few percent to more

than 10 % of the average oxygen concentration (Results section 3.4.2). Accordingly, it may be desirable to include a parameterization of these oxygen-poor and macronutrient-rich eddies in non-eddying models. We note that for such a *long-range*, regionally specific tracer flux, standard diffusion parameterizations may be only partially appropriate, as these typically exploit *local* tracer gradients [e.g., *Treguier et al.*, 2003]. Although these standard parameterization schemes can be applied to smear out local tracer gradients effectively, subsurface eddies act to spread smaller amounts of tracer non-locally over large distances. Given that there are no known non-local parameterizations of lateral tracer transport, we leave the development of a suitable parameterization approach to future studies.

In addition, the export of oxygen-poor waters from inshore to offshore regions by the eddies may, via mass conservation, facilitate the import of relatively oxygenated waters to the inshore regions [see also "Rossby rip currents" at the ocean surface, *Marshall et al.*, 2013]. It is possible that filaments occurring between eddies play an important role in this respect, as suggested by the visual impression of animations of oxygen on the 26.7 μmol kg^{-1} layer (see supplementary material sample animations) and the surface-ocean analysis of *Nagai et al.* [2015]. Results based on our model (Results section 3.4.3) suggest that Puddies are significant contributors to the "leakage" of poleward flowing undercurrents, particularly in the North Pacific. Accordingly, Puddies export low-oxygen waters from the undercurrents, becoming an intrinsic component of the processes that ventilate the subsurface EBUS. An opposite effect can be envisioned for macronutrients, whereby Puddies remove nutrient-rich subsurface waters that could otherwise be used to fuel productivity after upwelling. That is, formation and export of Puddies may be an integral component of

the "eddy quenching" of primary production in EBUS [*Gruber et al.*, 2011], with the difference that Puddies remove subsurface nutrients before they are exposed to the surface by upwelling.

4.2. Subsurface Coherent Eddies as *Hypoxic Storms* and *Stewpots*

Because of their efficient isolation from ambient waters, Puddies represent low-oxygen extreme events when they reach better-ventilated ambient waters (Results sections 3.3.2/3.4.1). For instance a suboxic subsurface coherent eddy has been observed at the Hawaii Ocean Time-series (HOT), several thousand kilometers offshore from its likely origin, the California poleward undercurrent [*Lukas and Santiago-Mandujano*, 2001]. In the model, Puddies account for a significant fraction of low-oxygen extreme events outside of suboxic waters along the isopycnal layers where they are found. This leads to the expectation of a similar contribution to low-oxygen processes such as denitrification and nitrous oxide production (*stewpot* effect). This effect of Puddies, combined with the spatial expansion of oxygen minimum zones by Puddies, may play a role in the lateral coupling of denitrification and nitrogen fixation [see e.g., *Landolfi et al.*, 2013].

It is possible that we underestimate the effect of subsurface coherent eddies on biogeochemical tracers for three reasons related to model physics. (i) The model resolution does not allow to simulate eddies much smaller than the first baroclinic Rossby radius, while with increasing model resolution, the number of subsurface coherent eddies approaching the submesoscale tends to increase [*Molemaker et al.*, 2015]. As smaller Puddies can propagate over similarly large distances while carrying extreme tracer anomalies [see e.g., *Lukas and Santiago-Mandujano*, 2001; *McWilliams*, 2016], we expect them to have similar effects as the larger ones. Our results should be considered indicative of mesoscale

Puddies, with the expectation that submesoscale Puddies will have additional impact. (ii) While we pick a certain density layer as representative for Puddies, $26.7\,\mathrm{kg}^{-3}$, we may miss the maximum anomaly of individual eddies if their core is slightly lighter or heavier, thereby overall underestimating eddy anomalies. (iii) Eddies in the model may be less coherent than in the real ocean given that the submesoscale processes which support the formation of subsurface mesoscale eddies via upscale flow self-organization [*Molemaker et al.*, 2015] are not included in the model used here.

In addition to these physical shortcomings of the model, Puddies in the model may underestimate the intensity of oxygen anomalies if they are missing an enhanced interior remineralization effect, as suggested by observations. Such an effect could arise from enhanced near-surface production [e.g., *Stramma et al.*, 2013; *Karstensen et al.*, 2015; *Schütte et al.*, 2016b], or by respiration of excess organic matter trapped by the eddies. This amplification effect may result in observed respiration rates within eddies several times as large as in surrounding waters [e.g., *Karstensen et al.*, 2015]. Hence, within a year one could expect an additional decrease of oxygen concentrations of several $10\,\mu\mathrm{mol\,kg}^{-1}$ in model eddies if enhanced respiration was well represented, i.e. an amplification of the low-oxygen anomalies and related transports. While the increased production above eddies (not shown) is captured by the model in some regions (the Atlantic), production appears damped in others (the Pacific). Furthermore, lateral transport of dissolved and suspended organic matter is not represented in the model, i.e. the *stewpot* effect is only partially resolved. Finally, another impact not accounted for by the model is potential behavioral changes of zooplankton and higher trophic levels due to the low-oxygen anomalies of Puddies, with potential implications for respiration and export [*Hauss et al.*, 2016]. This

possibility may have additional implications for the behaviour of large marine predators, including those targeted by fisheries.

5. Conclusions

We analyzed subsurface coherent eddies originating in the EBUS regions, here labeled *p*oleward *u*ndercurrent eddies, or "Puddies", in a global, eddying coupled climate model. The model simulates a rich and fairly realistic population of Puddies, as compared to the limited number of available in-situ observations and previous modeling studies. The model allows us to determine basin-wide statistics of Puddies, and provide a global estimate of their biogeochemical role. The latter has been hypothesized by several studies, but has never been quantified due to the paucity of observational data, and the lack of sufficiently high-resolution model results. The model we use provides an opportunity to fill the information gap. Given model biases (see Discussion section 4.2), we expect our estimate of the effects of Puddies on biogeochemical tracers to be conservative.

Our sample of Puddies comprises close to 10,000 eddies, all existing 3 months or longer, close to 10 % of which persist for 9 months or longer. At any given time, roughly 600 and 50 independent eddies with lifespans of 3 and 9 months, respectively, exist in the global ocean. Puddies tend to maintain strong coherence while propagating westward over distances of several hundred kilometers, and a few percent of them cover more than 1000 km over their lifetime. In the 1/10° model that we analyzed, they tend to occupy the mesoscale range, with average radii of around 50 km. Puddies carry physical and biogeochemical signatures typical of eastern boundary poleward undercurrents into the gyre interiors, where they appear as warm-salty anomalies, with the exception of the North Atlantic where they inherit a cold-fresh signature from the undercurrent. In all basins,

they tend to appear as low-oxygen, high-nutrient extreme events.

Puddies alter the characteristics of EBUS and adjacent waters, decreasing climatological oxygen levels along the boundary of EBUS and tropical oxygen minimum zones, exporting poleward undercurrent waters away from EBUS, and contributing to EBUS and subtropical gyre tracer budgets. These impacts are $\mathcal{O}$(1-10) %, with the largest effects being the "leakage" of waters from the undercurrents, and the associated offshore transport of biogeochemical tracers. Especially in the Pacific Ocean, the removal of nutrients by subsurface eddies is substantial, potentially contributing to the "eddy quenching" of productivity in the region [*Gruber et al.*, 2011], and, indirectly, to the ventilation of the oxygen minimum zones. We speculate that, due to the relative quiescence of the ocean interior and isolation from the air-sea interface, subsurface eddies maintain greater coherence than surface eddies, and are therefore particularly efficient at transporting material properties over long distances.

We conclude that, while not first order, Puddies contribute to shaping biogeochemical tracer distributions, exchanging properties between EBUS and the subtropical gyres. This exchange includes an important supply of oxygenated waters to the low oxygen regions. Additionally, by harboring low-oxygen processes in otherwise well-ventilated waters, they may affect greenhouse gas and macronutrient cycles and may represent an environmental feature that modifies the behaviour of water-breathing animals. Hence, depending on the question one pursues, they may deserve dedicated parameterizations in non-eddy resolving models. We have carried out our analysis with a focus on oxygen and macronutrients; similar conclusions should apply to other tracers.

Our quantitative assessment of Puddies and their biogeochemical effects is based on a

single model and should be regarded as a first, rather than a definitive estimate. It will be testable once comprehensive observed statistics of subsurface eddies, such as their formation and decay rate, and their biogeochemical signature, become available [e.g., for the North Atlantic see *Schütte et al.*, 2016b]. Conclusive assessments of eddy statistics and impacts, including their larger number and stronger effect in the Pacific compared to the Atlantic, and their role as "oasis" or "deserts" for higher trophic levels, will require large-scale observations and increased sampling of individual eddies, for example through distributed and autonomous observational networks such as Argo [e.g. *Zhang et al.*, 2017; *Li et al.*, 2017], or by gliders. Our results may serve as a guide for such dedicated observational efforts.

Acknowledgments. We are indebted to many scientists at NOAA GFDL for developing and providing access to the CM2.6 high-resolution model simulation. We thank Rena Czeschel and Lothar Stramma for providing the mooring data presented in Figure 2c, and Alexis Chaigneau and *Rudnick et al.* 2017 (data doi: 10.21238/S8SPRAY7292) for the undercurrent data presented in Figure 5. We thank Sören Thomsen for discussions and Stephen Griffies for valuable comments on the manuscript. D.B. acknowledges support from the U.S. National Science Foundation (NSF) grant OCE-1635414, and F.S. from the Collaborative Research Centre 754 (SFB 754) "Climate-Biogeochemistry Interactions in the Tropical Ocean", funded by the German Research Foundation (DFG).

The code of CM2.6 is based on ESM2M, available at https://www.gfdl.noaa.gov/earth-system-model, and includes the simple marine biogeochemical model miniBLING. Solutions from CM2.6 with its high resolution ocean component require large storage capacities. The solution analyzed here is available via the SOCCOM project upon request

(https://soccom.princeton.edu), and results of analyses of this project from the authors upon request.

References

Altabet, M. A., Ryabenko, E., Stramma, L., Wallace, D. W. R., Frank, M., Grasse, P., and Lavik, G. (2012), An eddy-stimulated hotspot for fixed nitrogen-loss from the Peru oxygen minimum zone, *Biogeosciences*, *9*, 4897–4908, doi:10.5194/bg-9-4897-2012.

Assassi, C., Y., Morel, F., Vandermeirsch, A., Chaigneau, C., Pegliasco, R., Morrow, F., Colas, S., Fleury, X., Carton, P., Klein, and R. Cambra (2016), An index to distinguish surface- and subsurface-intensified vortices from surface observations, *Journal of Physical Oceanography*, *46*, 2529–2552, doi:10.1175/JPO-D-15-0122.1.

Antonov, J. I., D. Seidov, T. P. Boyer, R. A. Locarnini, A. V. Mishonov, H. E. Garcia, O. K. Baranova, M. M. Zweng, and D. R. Johnson (2010), *World Ocean Atlas 2009, Volume 2: Salinity*, S. Levitus, Ed. NOAA Atlas NESDIS 69, U.S. Government Printing Office, Washington, D.C., 184 pp.

Arévalo-Martínez, D. L., A. Kock, C. R. Löscher, R. a. Schmitz, L. Stramma, and H. W. Bange (2016), Influence of mesoscale eddies on the distribution of nitrous oxide in the eastern tropical South Pacific, *Biogeosciences*, *13*, 1105–1118, doi:10.5194/bg-13-1105-2016.

Bashmachnikov, I., X., Carton, and T. V. Belonenko (2014), Characteristics of surface signatures of Mediterranean water eddies, *Journal of Geophysical Research: Oceans*, *119*, 7245–7266, doi:10.1002/2014JC010244.

Bianchi, D., E. D. Galbraith, D. A. Carozza, K. A. S. Mislan, and C. A. Stock (2013), Intensification of open-ocean oxygen depletion by vertically migrating animals, *Nature Geoscience*, *6*, 545–548, doi:10.1038/ngeo1837.

Bosse, A., Testor, P., Houpert, L., Damien, P., Prieur, L., Hayes, D., Taillandier, V., de Madron, X. D., d'Ortenzio, F., Coppola, L., Karstensen, J., and Mortier, L. (2016), Scales and dynamics of Submesoscale Coherent Vortices formed by deep convection in the northwestern Mediterranean Sea, *Journal of Geophysical Research: Oceans*, *120*, 7716–7742, doi:10.1002/2016JC012144.

Brandt, P., H. W. Bange, D. Banyte, M. Dengler, S. H. Didwischus, T. Fischer, R. J. Greatbatch, J. Hahn, T. Kanzow, J. Karstensen, A. Körtzinger, G. Krahmann, S. Schmidtko, L. Stramma, T. Tanhua, and M. Visbeck (2015), On the role of circulation and mixing in the ventilation of oxygen minimum zones with a focus on the eastern tropical North Atlantic, *Biogeosciences*, *12*, 489–512, doi:10.5194/bg-12-489-2015.

Chaigneau, A., N. Dominguez, G. Eldin, L. Vasquez, R. Flores, C. Grados, and V. Echevin (2013), Near-coastal circulation in the Northern Humboldt Current System from shipboard ADCP data, *Journal of Geophysical Research: Oceans*, *118*, 5251–5266, doi:10.1002/jgrc.20328.

Chelton, D. B., M. G. Schlax, and R. M. Samelson (2011), Global observations of nonlinear mesoscale eddies, *Progress in Oceanography*, *91*, 167–216, doi:10.1016/j.pocean.2011.01.002.

Ciani, I., D. (2017), Subsurface-intensified oceanic vortices: impact on the sea-surface and mutual interactions, *PhD thesis*. Retrieved from https://tel.archives-ouvertes.fr/tel-01481211. Brest, Université de Bretagne occidentale.

Collins, C. a., T. Margolina, T. a. Rago, and L. Ivanov (2013), Looping RAFOS floats in the California Current System, *Deep-Sea Research Part II: Topical Studies in Oceanography*, *85*, 42–61, doi:10.1016/j.dsr2.2012.07.027.

Combes, V., Hormazabal, S., and Di Lorenzo, E. (2015), Interannual variability of the subsurface eddy field in the Southeast Pacific, *Journal of Geophysical Research: Oceans*, *120*, 4907–4924, doi:10.1002/2014JC010265.

Condie, S. A., and J. R. Dunn (2006), Seasonal characteristics of the surface mixed layer in the Australasian region: Implications for primary production regimes and biogeography, *Marine and Freshwater Research*, *57*, 569–590, doi:10.1071/MF06009.

D'Asaro, E. A. (1988), Generation of submesoscale vortices: A new mechanism, *Journal of Geophysical Research*, *93*(C6), 6685–6693, doi:10.1029/JC093iC06p06685.

Dewar, W. K., J. C. McWilliams, M. J. Molemaker, W. K. Dewar, J. C. McWilliams, and M. J. Molemaker (2015), Centrifugal instability and mixing in the California Undercurrent, *Journal of Physical Oceanography*, *45*, 1224–1241, doi:10.1175/JPO-D-13-0269.1.

Dufour, C. O., S. M. Griffies, G. F. de Souza, I. Frenger, A. K. Morrison, J. B. Palter, J. L. Sarmiento, E. D. Galbraith, J. P. Dunne, W. G. Anderson, and R. D. Slater (2015), Role of mesoscale eddies in cross-frontal transport of heat and biogeochemical tracers in the Southern Ocean, *Journal of Physical Oceanography*, *45*, 3057–3081, doi:10.1175/JPO-D-14-0240.1.

Faghmous, J. H., I. Frenger, Y. Yao, R. Warmka, A. Lindell, and V. Kumar (2015), A daily global mesoscale ocean eddy dataset from satellite altimetry, *Scientific Data*, *2*, Article number: 150028, doi:10.1038/sdata.2015.28.

Frenger, I., M. Münnich, N. Gruber, and R. Knutti (2015), Southern Ocean eddy phenomenology, *Journal of Geophysical Research: Oceans*, *120*, 7413–7449, doi: 10.1002/2015JC011047.

Galbraith, E. D., J. P. Dunne, A. Gnanadesikan, D. Richard, J. L. Sarmiento, C. O. Dufour, F. Gregory, D. Bianchi, M. Claret, and K. B. Rodgers (2015), Complex functionality with minimal computation: Promise and pitfalls of reduced-tracer ocean biogeochemistry models, *Journal of Advances in Modeling Earth Systems*, , *7*, 2012–2028, doi:10.1002/2015MS000463.

Garcia, H. E., R. A. Locarnini, T. P. Boyer, J. I. Antonov, O. K. Baranova, M. M. Zweng, and D. R. Johnson (2010a), *World Ocean Atlas 2009, Volume 3: Dissolved Oxygen, Apparent Oxygen Utilization, and Oxygen Saturation*, S. Levitus, Ed. NOAA Atlas NESDIS 70, U.S. Government Printing Office, Washington, D.C., 344 pp.

Garcia, H. E., R. A. Locarnini, T. P. Boyer, J. I. Antonov, M. M. Zweng, O. K. Baranova, and D. R. Johnson (2010b), *World Ocean Atlas 2009, Volume 4: Nutrients (phosphate, nitrate, silicate)*, S. Levitus, Ed. NOAA Atlas NESDIS 71, U.S. Government Printing Office, Washington, D.C., 398 pp.

Gnanadesikan, A., A. M. De Boer, and B. K. Mignone (2007), A simple theory of the pycnocline and overturning revisited, in *Ocean Circulation: Mechanisms and Impacts - Past and Future Changes of Meridional Overturning* (eds A. Schmittner, J. C. H. Chiang and S. R. Hemming), American Geophysical Union, Washington, D. C.. doi: 10.1029/173GM04.

Griffies, S. M., M. Winton, W. G. Anderson, R. Benson, T. L. Delworth, C. O. Dufour, J. P. Dunne, P. Goddard, A. K. Morrison, A. Rosati, A. T. Wittenberg, J. Yin, and

R. Zhang (2015), Impacts on ocean heat from transient mesoscale eddies in a hierarchy of climate models, *Journal of Climate*, *28*, 952–977, doi:10.1175/JCLI-D-14-00353.1.

Griffies, S. M., G. Danabasoglu, P. J. Durack, A. J. Adcroft, V. Balaji, C. W. Böning, E. P. Chassignet, E. Curchitser, J. Deshayes, H. Drange, B. Fox-Kemper, P. J. Gleckler, J. M. Gregory, H. Haak, R. W. Hallberg, H. T. Hewitt, D. M. Holland, T. Ilyina, J. H. Jungclaus, Y. Komuro, J. P. Krasting, W. G. Large, S. J. Marsland, S. Masina, T. J. McDougall, A. J. G. Nurser, J. C. Orr, A. Pirani, F. Qiao, R. J. Stouffer, K. E. Taylor, A. M. Treguier, H. Tsujino, P. Uotila, M. Valdivieso, M. Winton, and S. G. Yeager (2016), OMIP contribution to CMIP6: experimental and diagnostic protocol for the physical component of the Ocean Model Intercomparison Project, *Geoscientific Model Development*, *9*, 3231–3296, doi:10.5194/gmd-9-3231-2016.

Gruber, N., Z. Lachkar, H. Frenzel, P. Marchesiello, M. Münnich, J. C. McWilliams, T. Nagai, and G.-K. Plattner (2011), Eddy-induced reduction of biological production in eastern boundary upwelling systems, *Nature Geoscience*, *4*, 787–792, doi:10.1038/ngeo1273.

Grundle, D. S., Löscher, C. R., Krahmann, G., Altabet, M. A., Bange, H. W., Karstensen, J., Körtzinger, A., and Fiedler, B. (2017), Low oxygen eddies in the eastern tropical North Atlantic: Implications for N_2O cycling., *Scientific Reports*, *7*, 4806, doi:10.1038/s41598-017-04745-y.

Gula, J., M. J. Molemaker, J. C. McWilliams, J. Lilly, and L. N. Thomas (2016), Topographic generation of submesoscale centrifugal instability and energy dissipation, *Nature Communications*, *7*, Article number: 12811, doi:10.1038/ncomms12811.

Hallberg, R. (2013), Using a resolution function to regulate parameterizations of oceanic mesoscale eddy effects, *Ocean Modelling*, *72*, 92–103, doi:10.1016/j.ocemod.2013.08.007.

Haller, G. (2015), Lagrangian Coherent Structures, *Annual Review of Fluid Mechanics*, *47*, 137–162, doi:10.1146/annurev-fluid-010313-141322.

Hauss, H., S. Christiansen, F. Schütte, R. Kiko, M. Edvam Lima, E. Rodrigues, J. Karstensen, C. R. Löscher, A. Körtzinger, and B. Fiedler (2016), Dead zone or oasis in the open ocean? Zooplankton distribution and migration in low-oxygen modewater eddies, *Biogeosciences*, *13*, 1977–1989, doi:10.5194/bg-13-1977-2016.

Hormazabal, S., Combes, V., Morales, C. E., Correa-Ramirez, M. A., Di Lorenzo, E., and Nuñez, S. (2013), Intrathermocline eddies in the coastal transition zone off central Chile (31–41°), *Journal of Geophysical Research: Oceans*, *118*, 4811–4821,doi: 10.1002/jgrc.20337.

Johnson, G. C., and K. E. McTaggart (2010), Equatorial Pacific 13°C water eddies in the eastern subtropical South Pacific Ocean, *Journal of Physical Oceanography*, *40*, 226–236, doi:10.1175/2009JPO4287.1.

Karstensen, J., B. Fiedler, F. Schütte, P. Brandt, A. Körtzinger, G. Fischer, R. Zantopp, J. Hahn, M. Visbeck, and D. Wallace (2015), Open ocean dead zones in the tropical North Atlantic Ocean, *Biogeosciences*, *12*, 2597–2605, doi:10.5194/bg-12-2597-2015.

Key, R. M., A. Kozyr, C. L. Sabine, K. Lee, R. Wanninkhof, J. L. Bullister, R. A. Feely, F. J. Millero, C. Mordy, and T.-H. Peng (2004), A global ocean carbon climatology: Results from Global Data Analysis Project (GLODAP), *Global Biogeochemical Cycles*, *18*, GB4031, doi:10.1029/2004GB002247.

Kurian, J., F. Colas, X. Capet, J. C. McWilliams, and D. B. Chelton (2011), Eddy properties in the California Current System, *Journal of Geophysical Research*, *116*, C08027, doi:10.1029/2010JC006895.

Landolfi, A., H. Dietze, W. Koeve, and A. Oschlies (2013), Overlooked runaway feedback in the marine nitrogen cycle: the vicious cycle, *Biogeosciences*, *10*, 1351–1363, doi: 10.5194/bg-10-1351-2013.

Li, C., Zhang, Z., Zhao, W., and Tian, J. (2017), A statistical study on the subthermocline submesoscale eddies in the northwestern Pacific Ocean based on Argo data, *Journal of Geophysical Research: Oceans*, *122*, 3586–3598, doi:10.1002/2016JC012561.

Locarnini, R. A., A. V. Mishonov, J. I. Antonov, T. P. Boyer, H. E. Garcia, O. K. Baranova, M. M. Zweng, and D. R. Johnson (2010), *World Ocean Atlas 2009, Volume 1: Temperature*, S. Levitus, Ed. NOAA Atlas NESDIS 68, U.S. Government Printing Office, Washington, D.C., 184 pp.

Löscher, C. R., Fischer, M. A., Neulinger, S. C., Fiedler, B., Philippi, M., Schütte, F., Singh, A., Hauss, H., Karstensen, J., Körtzinger, A., Künzel, S., and Schmitz, R. A. (2015), Hidden biosphere in an oxygen-deficient Atlantic open-ocean eddy: future implications of ocean deoxygenation on primary production in the eastern tropical North Atlantic, *Biogeosciences*, *12*, 7467–7482, doi:0.5194/bg-12-7467-2015.

Lukas, R., and F. Santiago-Mandujano (2001), Extreme water mass anomaly observed in the Hawaii ocean time-series, *Geophysical Research Letters*, *28*, 2931–2934, doi: 10.1029/2001GL013099.

Marshall, D. P., B. Vogel, and X. Zhai (2013), Rossby rip currents, *Geophysical Research Letters*, *40*, 4333–4337, doi:10.1002/grl.50842.

McWilliams, J. C. (1985), Submesoscale, coherent vortices in the ocean, *Reviews of Geophysics*, *23*, 165–182, doi:10.1029/RG023i002p00165.

McWilliams, J. C. (2016), Submesoscale currents in the ocean. *Proceedings of the Royal Society of London A: Mathematical, Physical and Engineering Sciences*, *472:20160117*, doi:10.1098/rspa.2016.0117.

Molemaker, M. J., J. C. McWilliams, and W. K. Dewar (2015), Submesoscale generation of mesoscale anticyclones near a separation of the California Undercurrent, *Journal of Physical Oceanography*, *45*, 613–629, doi:10.1175/JPO-D-13-0225.1.

Morales, C. E., S. Hormazabal, M. Correa-Ramirez, O. Pizarro, N. Silva, C. Fernandez, V. Anabalón, and M. L. Torreblanca (2012), Mesoscale variability and nutrient-phytoplankton distributions off central-southern Chile during the upwelling season: The influence of mesoscale eddies, *Progress in Oceanography*, *104*, 17–29,doi: 10.1016/j.pocean.2012.04.015.

Nagai, T., N. Gruber, H. Frenzel, J. C. Mcwilliams, and G. Plattner (2015), Dominant role of eddies in the offshore transport of carbon and nutrients in the California Current System, *Journal of Geophysical Research*, *120*, 5318–5341, doi:10.1002/2015JC010889.

Okubo, A. (1970), Horizontal dispersion of floatable particles in the vicinity of velocity singularities such as convergences, *Deep-Sea Research*, *17*, 445–454, doi:10.1016/0011-7471(70)90059-8.

Pegliasco, C., A. Chaigneau, and R. Morrow (2015), Main eddy vertical structures observed in the four major Eastern Boundary Upwelling Systems, *Journal of Geophysical Research: Oceans*, *120*, 6008–6033, doi:10.1002/2015JC010950.

Pelland, N. A., C. C. Eriksen, and C. M. Lee (2013), Subthermocline eddies over the Washington continental slope as observed by seagliders, 2003-09, *Journal of Physical Oceanography*, *43*, 2025–2053, doi:10.1175/jpo-d-12-086.1.

Riser, S.C., W.B. Owens, H.T. Rossby, and C.C. Ebbesmeyer (1986), The structure, dynamics, and origin of a small-scale lens of water in the western North Atlantic thermocline, *Journal of Physical Oceanography*, *16*, 572–590, doi:10.1175/1520-0485(1986)016¡0572:TSDAOO¿2.0.CO;2.

Rudnick, D. L., Zaba, K. D., Todd, R. E., and Davis, R. E. (2017), A climatology of the California Current System from a network of underwater gliders, *Progress in Oceanography*, *154*, 64–106, doi:10.1016/j.pocean.2017.03.002.

Schütte, F., P. Brandt, and J. Karstensen (2016a), Occurrence and characteristics of mesoscale eddies in the tropical northeastern Atlantic Ocean, *Ocean Science*, *12*, 663–685, doi:10.5194/os-12-663-2016.

Schütte, F., J. Karstensen, G. Krahmann, H. Hauss, B. Fiedler, P. Brandt, M. Visbeck, and A. Körtzinger (2016b), Characterization of "dead-zone" eddies in the eastern tropical North Atlantic, *Biogeosciences*, *13*, 5865–5881, doi:10.5194/BG-13-5865-2016.

Solodoch, A., Stewart, A. L., and McWilliams, J. C. (2016), Baroclinic instability of axially symmetric flow over sloping bathymetry, *Journal of Fluid Mechanics*, *799*, 265–296, doi:10.1017/jfm.2016.376.

Stramma, L., E. D. Prince, S. Schmidtko, J. Luo, J. P. Hoolihan, M. Visbeck, D. W. R. Wallace, P. Brandt, and A. Körtzinger (2011), Expansion of oxygen minimum zones may reduce available habitat for tropical pelagic fishes, *Nature Climate Change*, *2*, 33–37, doi:10.1038/nclimate1304.

Stramma, L., H. W. Bange, R. Czeschel, A. Lorenzo, and M. Frank (2013), On the role of mesoscale eddies for the biological productivity and biogeochemistry in the eastern tropical Pacific Ocean off Peru, *Biogeosciences*, *10*, 7293–7306, doi:10.5194/bg-10-7293-

2013.

Stramma, L., R. A. Weller, R. Czeschel, and S. Bigorre (2014), Eddies and an extreme water mass anomaly observed in the eastern South Pacific at the Stratus mooring, *Journal of Geophysical Research: Oceans*, *119*, 1068–1083, doi:10.1002/2013JC009470.

Thomsen, S. (2016), The formation of a subsurface anticyclonic eddy in the Peru-Chile Undercurrent and its impact on the near-coastal salinity, oxygen, and nutrient distributions, *Journal of Geophysical Research: Oceans*, *121*, 476–501 doi:10.1002/2015JC010878.

Treguier, A., O. Boebel, B. Barnier, and G. Madec (2003), Agulhas eddy fluxes in a 1/6° Atlantic model, *Deep Sea Research Part II: Topical Studies in Oceanography*, *50*, 251–280, doi:10.1016/S0967-0645(02)00396-X.

Weiss, J. (1991), The dynamics of enstrophy transfer in two-dimensional hydrodynamics, *Physica D: Nonlinear Phenomena*, *48*(2-3), 273–294, doi:10.1016/0167-2789(91)90088-Q.

Zhang, Z., Y. Zhang, and W. Wang (2017), Three-compartment structure of subsurface-intensified mesoscale eddies in the ocean, *Journal of Geophysical Research: Oceans*, *122*, 1653–1664, doi:10.1002/2016JC012376.

Table 1. Overview of Puddy characteristics (mean, in brackets the 10^{th} and 90^{th} percentiles)

Region	Lifespan [months]	Radius [km]	Propagation speed[a] [km day^{-1}]	Lifespan [months]	Propagation distance [km]
All	≥3	52 (27/84)	2.6 (0.4/4.9)	6 (3/9)	313 (81/607)
	≥9	61 (32/92)	2.5 (0.8/4.5)	15 (9/25)	848 (262/1580)
North Atlantic	≥3	52 (29/83)	2.7 (0.2/5.1)	5 (3/7)	258 (78/486)
	≥9	60 (33/89)	2.9 (0.7/5.2)	11 (9/13)	714 (317/1173)
South Atlantic	≥3	54 (29/87)	2.9 (0.5/5.2)	5 (3/8)	349 (104/615)
	≥9	65 (36/95)	3.2 (1.0/5.3)	13 (9/20)	1059 (347/2012)
North Pacific	≥3	49 (26/79)	2.3 (0.4/4.3)	6 (3/10)	284 (70/580)
	≥9	57 (31/85)	2.1 (0.7/3.8)	16 (10/29)	727 (214/1310)
South Pacific	≥3	55 (28/93)	2.8 (0.5/5.1)	5 (3/8)	347 (90/658)
	≥9	67 (35/105)	2.9 (1.0/4.5)	14 (9/21)	988 (372/1764)

[a]Includes advection by ambient flow.

Table 2. Overview of Puddy physical and biogeochemical tracer extrema (mean, in brackets the 10^{th} and 90^{th} percentiles), i.e. at the center of Puddies, relative to climatological values on the $26.7\,\mathrm{kg\,m^{-3}}$ isopycnal layer

Region	Lifespan [months]	ΔTemperature [C°]	ΔSalinity [psu]	ΔOxygen [μmol kg^{-1}]	ΔMacronutrient [μmol kg^{-1}]
All	≥3	+0.1 (-0.1/+0.5)	+0.03 (-0.02/+0.11)	-17 (-50/+8)	+0.13 (-0.12/+0.44)
	≥9	+0.3 (0.0/+0.9)	+0.06 (0.00/+0.19)	-36 (-84/-1)	+0.27 (-0.01/+0.64)
North Atlantic	≥3	-0.3 (-1.0/+0.3)	-0.08 (-0.27/+0.07)	-7 (-36/+19)	+0.12 (-0.26/+0.53)
	≥9	-0.4 (-1.2/+0.2)	-0.10 (-0.32/+0.05)	-13 (-46/+14)	+0.18 (-0.21/+0.69)
South Atlantic	≥3	+0.1 (0.0/+0.2)	+0.01 (-0.01/+0.04)	-17 (-57/+10)	+0.15 (-0.14/+0.53)
	≥9	+0.1 (0.0/+0.2)	+0.02 (-0.01/+0.04)	-41 (-100/+4)	+0.38 (-0.08/+1.00)
North Pacific	≥3	+0.2 (-0.1/+0.4)	+0.03 (-0.01/+0.08)	-14 (-38/+2)	+0.13 (-0.04/+0.37)
	≥9	+0.3 (0.0/+0.5)	+0.05 (0.00/+0.09)	-24 (-47/-2)	+0.23 (0.00/+0.49)
South Pacific	≥3	+0.3 (-0.1/+0.9)	+0.06 (-0.01/+0.19)	-23 (-79/+14)	+0.11 (-0.19/+0.48)
	≥9	+0.7 (+0.2/+1.2)	+0.15 (+0.03/+0.25)	-61 (-117/-9)	+0.34 (-0.02/+0.79)

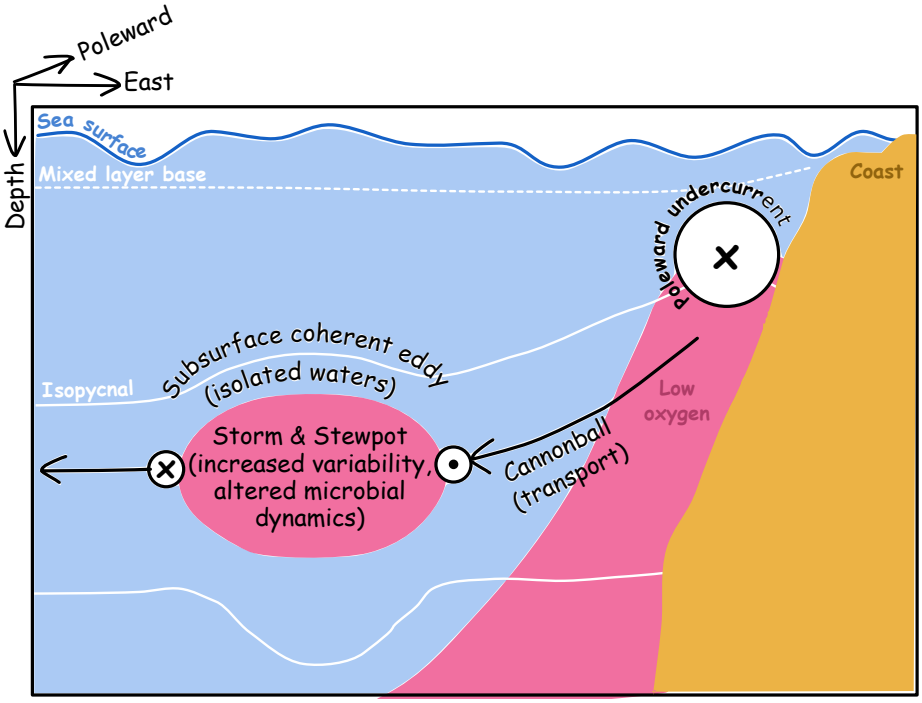

Figure 1. Schematic of the biogeochemical effects of subsurface coherent eddies originating in eastern boundary upwelling systems, referred to as *p*oleward *u*ndercurrent eddies (Puddies) in the paper; here shown for the northern hemisphere.

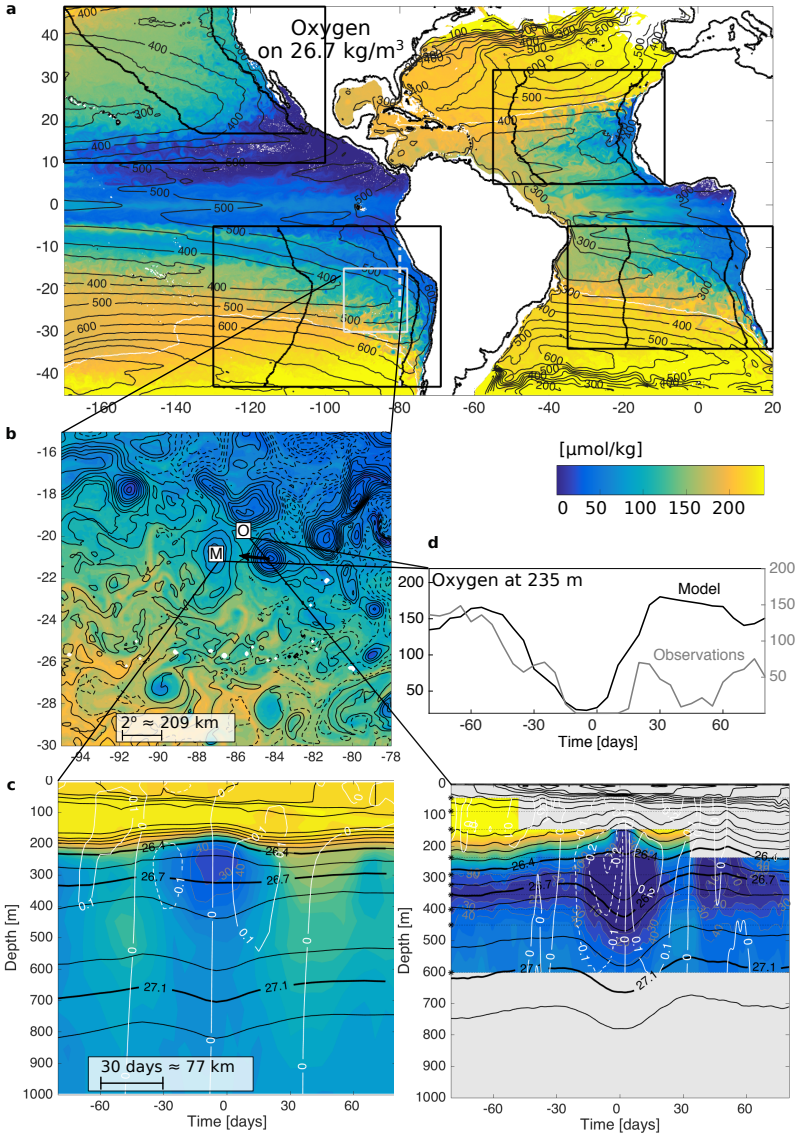

Figure 2. Region of study and sample Puddies. (a) Model snapshot (5-day average) of oxygen (colors) on an isopycnal layer (26.7 kg m^{-3}, note that the layer outcrops and does not extent to the coast in all places), with the climatological 200 µmol kg^{-1} contour overlayed in light gray, and the thickness of the 27.1 - 26.4 kg m^{-3} layer overlayed in black (50 m intervals). The four black boxes indicate the focus regions of the study, and the black lines following the shape of the coastlines the regions used for the calculation of transports (Methods section 2.4.1). The vertical white dashed line in the South Pacific denotes one of the meridional sections used to assess the density range of eddies (see Figure 3b and Methods section 2.3.1), the black box the inset shown in (b). (b) Colors show the same as in (a), black contours layer thickness *anomalies* (10 m intervals, solid: positive, dashed: negative) used for the detection of Puddies; white squares indicate geographical locations for the model **M** and for an observational mooring **O**, and the black arrow marks the eddy which will pass by M. (c) Time series (160 days) of oxygen extracted from the model (M) (left panel), and a vertically interpolated time series at the mooring O (reproduced from *Stramma et al.*, 2014). Oxygen is shown in colors (gray indicates lack of observations, asterisks indicate depths of measurements), densities as black contours and the meridional velocity as white contours. (d) The same oxygen time series as in (c) at the approximate core of the eddies, 235 m; the observational time series is averaged over 5 day intervals to match the model resolution; the vertical axes have the same range but are slightly shifted to simplify a visual comparison of the magnitude of the oxygen drop associated with the eddies.

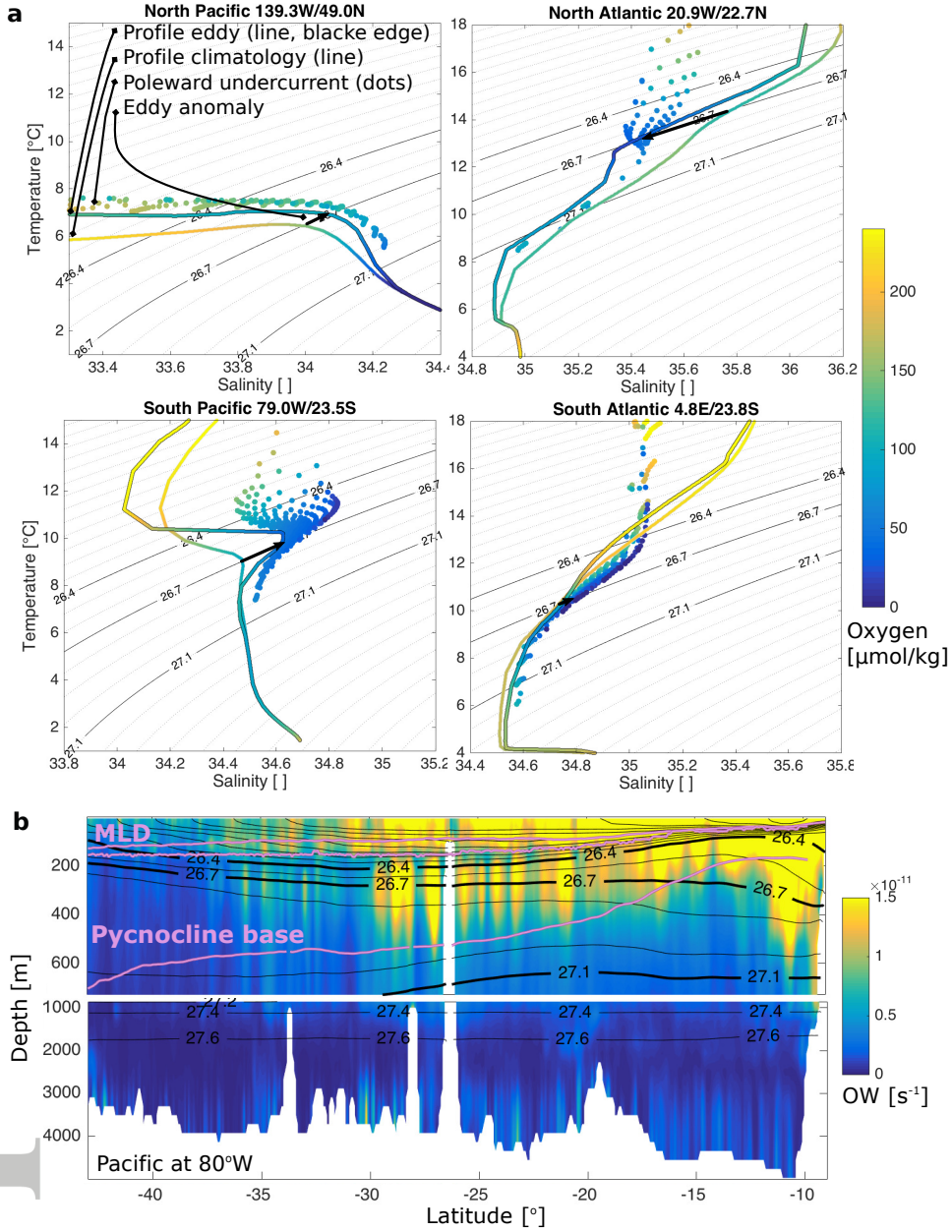

Figure 3. Density range and hydrographic properties of Puddies. (a) Temperature-salinity diagrams showing: profiles of representative eddies from each of the focus regions, climatological profiles at the same location, and the characteristics of poleward undercurrent waters within 500 km off the coast with flow greater than 1 cm s^{-1} down to 500 m (dots). Colors indicate oxygen concentrations. (b) Meridional section of the temporal standard deviation of the Okubo-Weiss parameter over years 181 - 200, here for the South Pacific at 80°W (see dashed white line in Figure 2a). Black contours indicate selected densities; purple contours from the surface to the bottom: the maximum of the climatological monthly mixed layer (MLD), the maximum vertical density gradient in the pycnocline and the pycnocline base defined as the minimum MLD plus the pycnocline thickness [*Gnanadesikan et al.*, 2007, equation (6)].

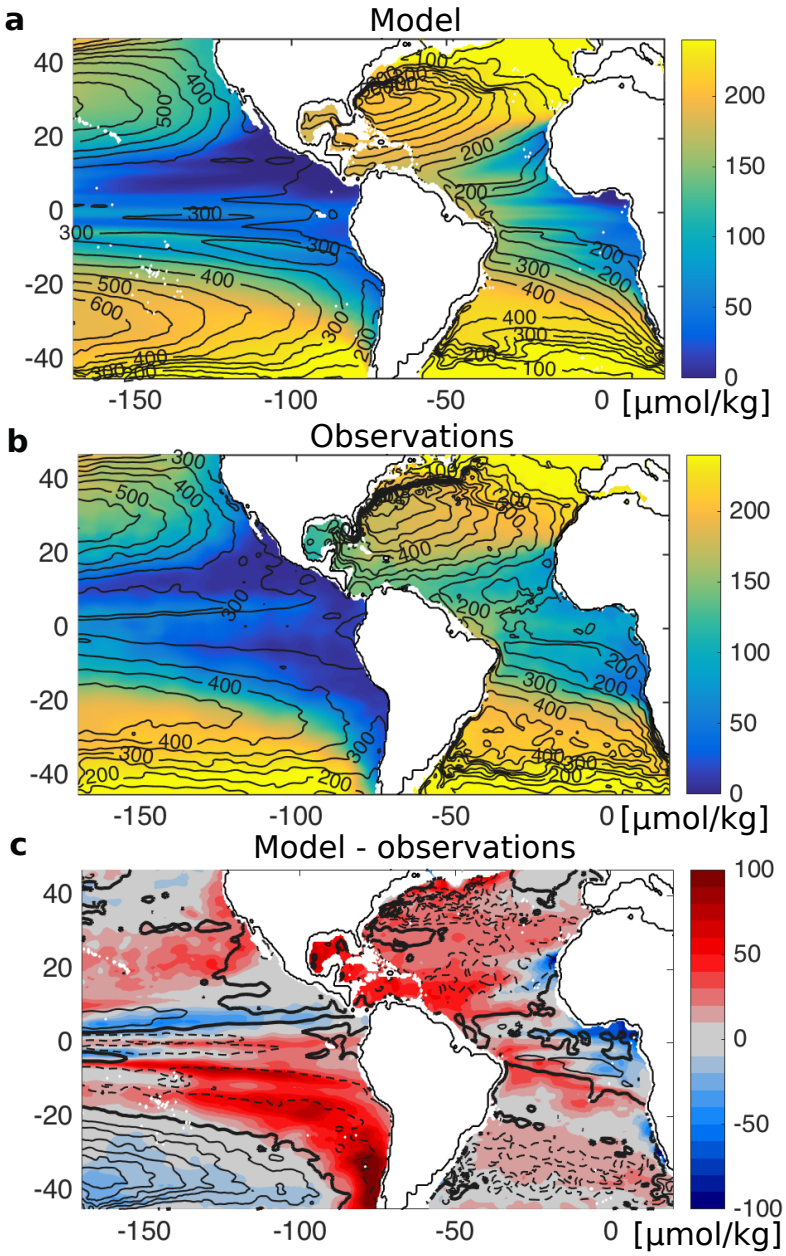

Figure 4. Comparison of model and observed oxygen concentration (colors) and depth of the isopycnal layer of Puddies (26.7 kg m^{-3}). (a) Model; (b) observations [CARS, *Condie and Dunn*, 2006]; and (c) difference (a-b). Depth anomalies in (c) are indicated in solid if positive, i.e. deeper, and dashed if negative, i.e. shallower. Intervals are 50 m, the zero-isoline is shown in bold.

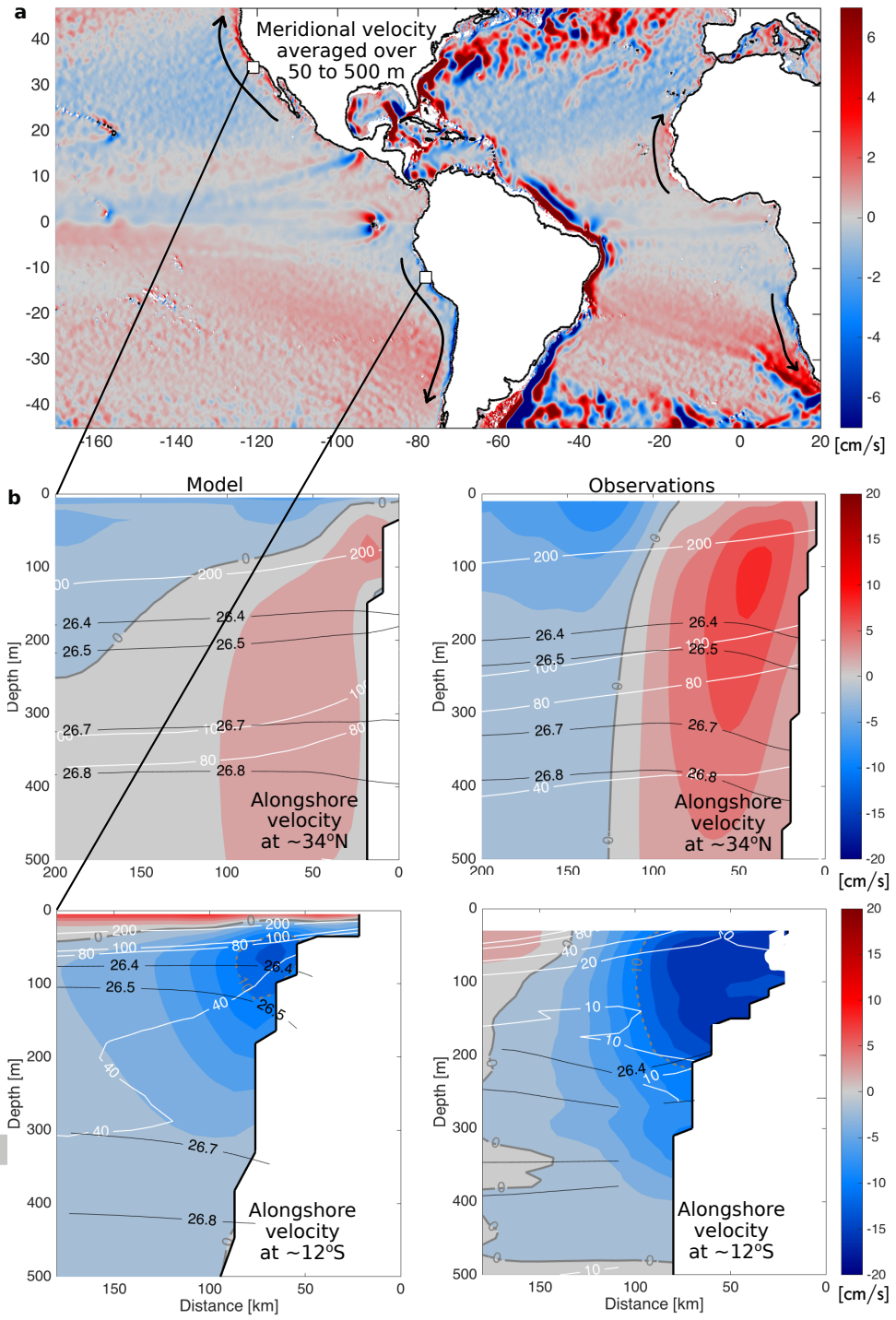

Figure 5. Model representation of eastern boundary poleward undercurrents. (a) Vertical average (50 to 500 m) of the meridional velocity component in the model; arrows indicate the undercurrents; white squares mark the sections shown in (b), i.e. climatological alongshore velocity (colors) in the model (left panels) compared to temporally averaged in-situ observations at approximately the same locations (right panels, from *Rudnick et al.*, 2017, for the North Pacific, and *Chaigneau et al.*, 2013, for the South Pacific). Gray contours in (b) denote selected velocity levels, black contours selected density layers, and white contours selected oxygen levels. Note the lack of observations near the ocean surface.

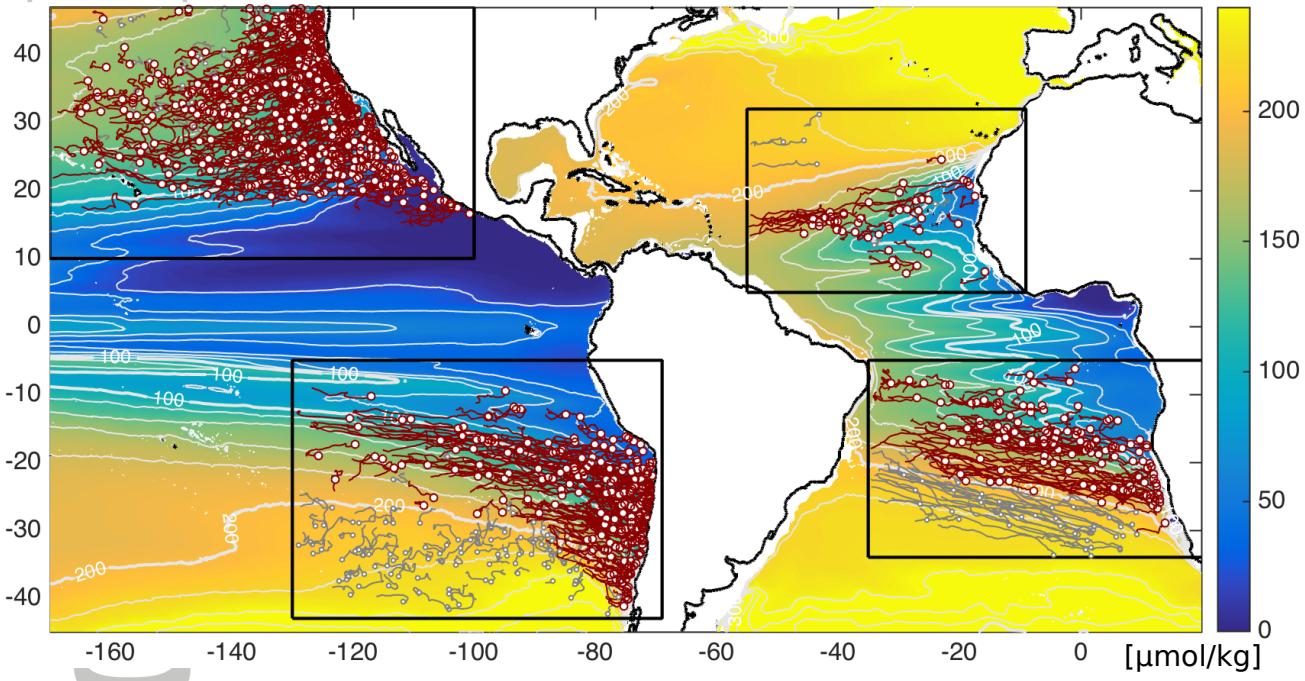

Figure 6. Tracks of Puddies existing 9 months or longer. Grey and red lines show the tracks of all tracked eddies, red lines indicate the analyzed subsample of eddies with a net westward propagation that originate in waters with climatological oxygen below 200 µmol kg^{-1}; white dots mark the origin (first detection) of individual eddies; the background shows climatological oxygen concentrations (colors) on the isopycnal layer of Puddies (26.7 µmol kg^{-1}); white contours and labels mark selected oxygen levels; black boxes indicate the analysis regions.

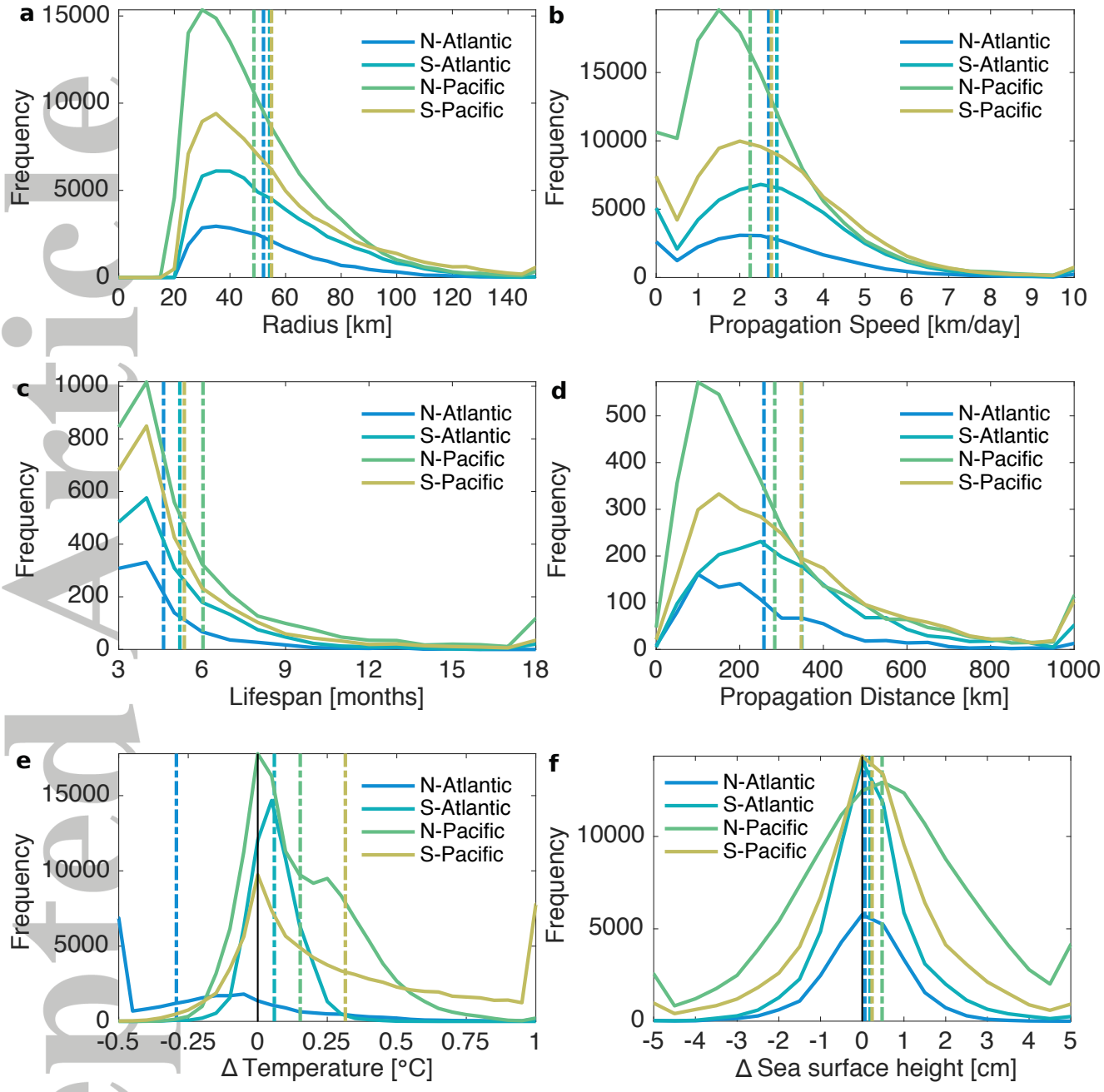

Figure 7. Characteristics of Puddies existing 3 months or longer. Histograms show the frequency distributions of: (a) the eddy radius (5 km bins); (b) eddy propagation speeds (0.5 km day^{-1} bins); (c) eddy lifespans (1 month bins); (d) distances eddies cover over their lifetime (100 km bins); (e) temperature anomalies at the center of eddies (0.05 °C bins, on 26.7 kg m^{-3}); the distribution of salinity anomalies has the same shape due to density compensation); and (f) sea surface height anomalies (0.05 cm bins). Note that the frequency increase at the tails of the distributions is due to the outermost bins containing all instances "smaller (left tail) or larger (right tail) than". Vertical dashed lines denote the means; colors indicate the four focus regions; only eddies with a net westward propagation and which originate in climatological oxygen concentrations lower than 200 µmol kg^{-1} are considered.

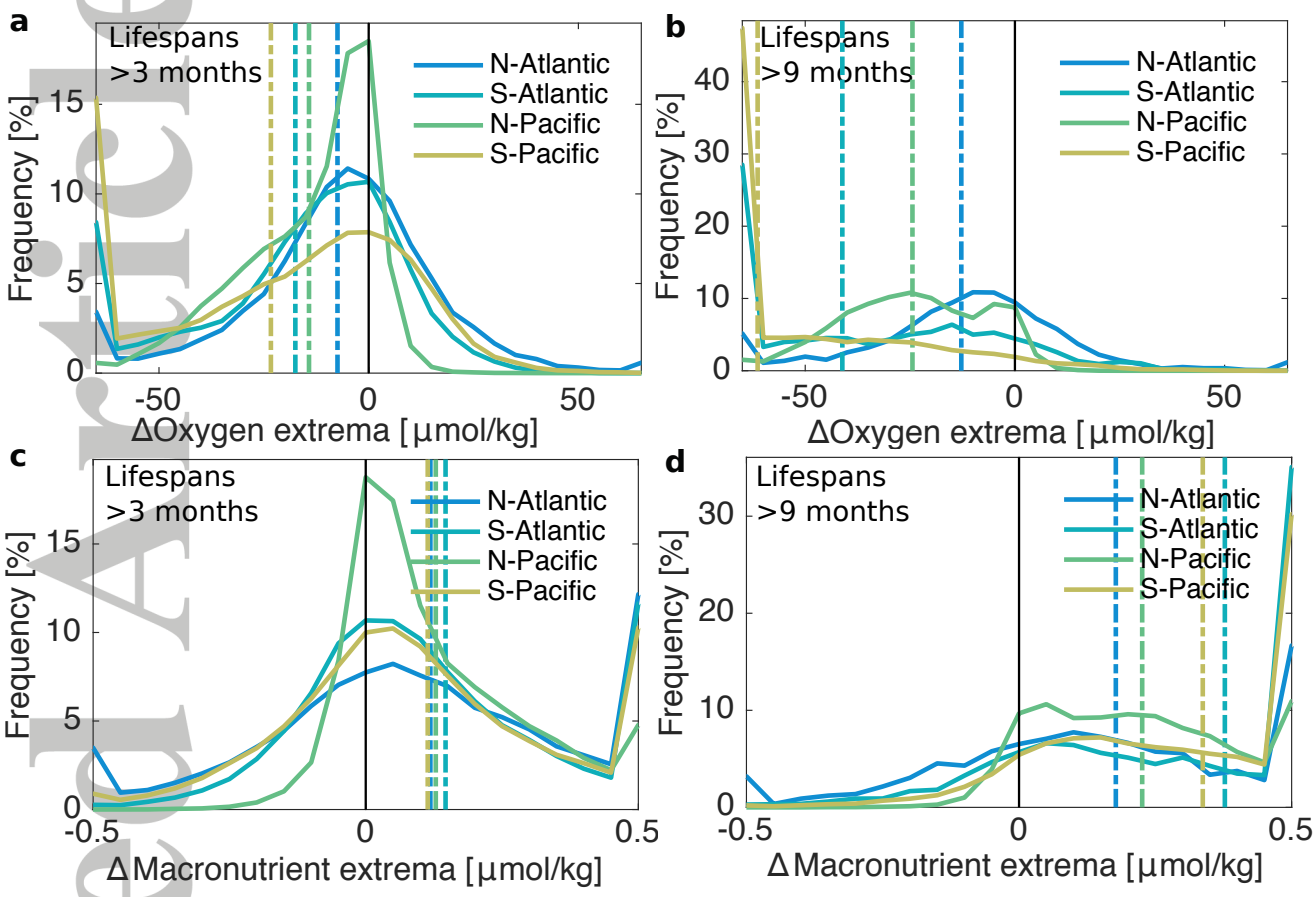

Figure 8. Biogeochemical characteristics of Puddies. The histograms show the frequency distributions of tracer anomaly at the center, i.e. extrema, of Puddies existing (a,c) 3 months or longer and (b,d) 9 months or longer (using 5 µmol kg^{-1} and 0.05 µmol kg^{-1} bins for oxygen and the general macronutrient, respectively). Vertical dashed lines denote the means; colors indicate the four focus regions; only eddies with a net westward propagation and which originate in climatological oxygen conditions lower than 200 µmol kg^{-1} are considered.

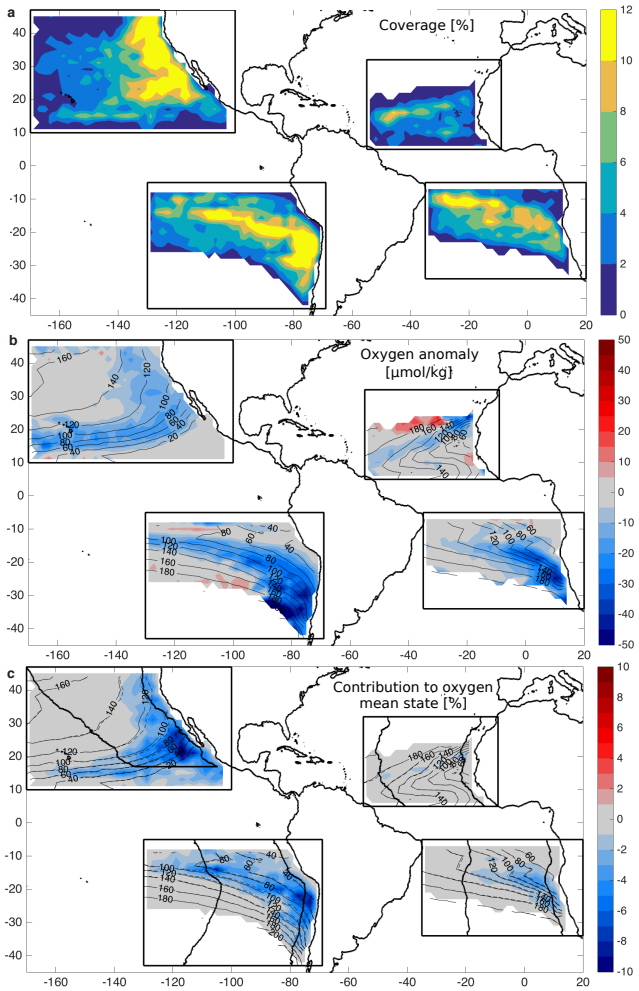

Figure 9. Effect of Puddies on the mean oxygen distribution. (a) Fractional coverage by Puddies existing 3 months or longer, propagating westward and originating in climatological oxygen conditions lower than 200 µmol kg^{-1}, based on regridding to 2×2 longitude-latitude boxes. (b) Average oxygen anomalies of the same eddies regridded to 2×2 longitude-latitude boxes on the isopycnal layer of the eddy cores (26.7 µmol kg^{-1}). (c) Reduction of climatological oxygen due to the presence of Puddies on the same isopycnal layer, relative to the climatological oxygen field if the eddies did not exist (see text, shown as dashed black contours). Solid black lines in (b,c) show the actual climatological oxygen, indicating an offshore expansion of oxygen minimum zones arising from the eddies; black boxes indicate the analysis regions; lines parallel to the coast in (c) show the inshore (500 km) and offshore (4000 km) regions used for the assessment of the biogeochemical tracer budget (Figure 12).

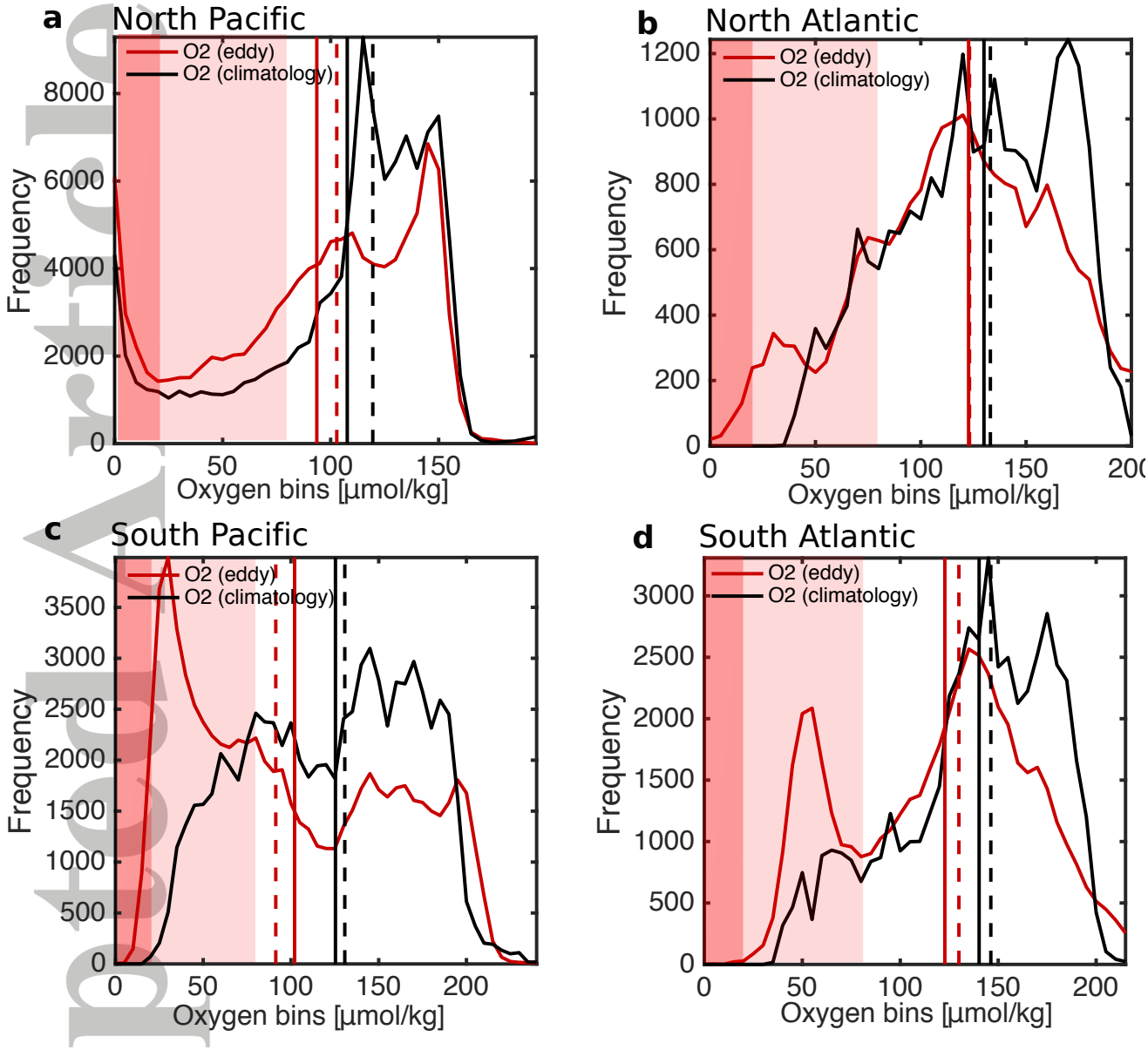

Figure 10. Puddies as low-oxygen extreme events. Red lines show the frequency distribution of oxygen (O2) at the center of Puddies, i.e. extreme values, on the isopycnal layer of the eddy cores (26.7 μmol kg^{-1}, 5 μmol kg^{-1} bins); black lines the frequency distribution of climatological oxygen at the eddy centers. Distributions are calculated in the (a) North Pacific, (b) North Atlantic, (c) South Pacific and (d) South Atlantic, for eddies with lifespans of at least 3 months; vertical bars indicate the means (solid) and medians (dashed); red shadings indicate 80 (pale) and 20 (dark) μmol kg^{-1} oxygen levels, here taken as thresholds for hypoxic and suboxic conditions, respectively.

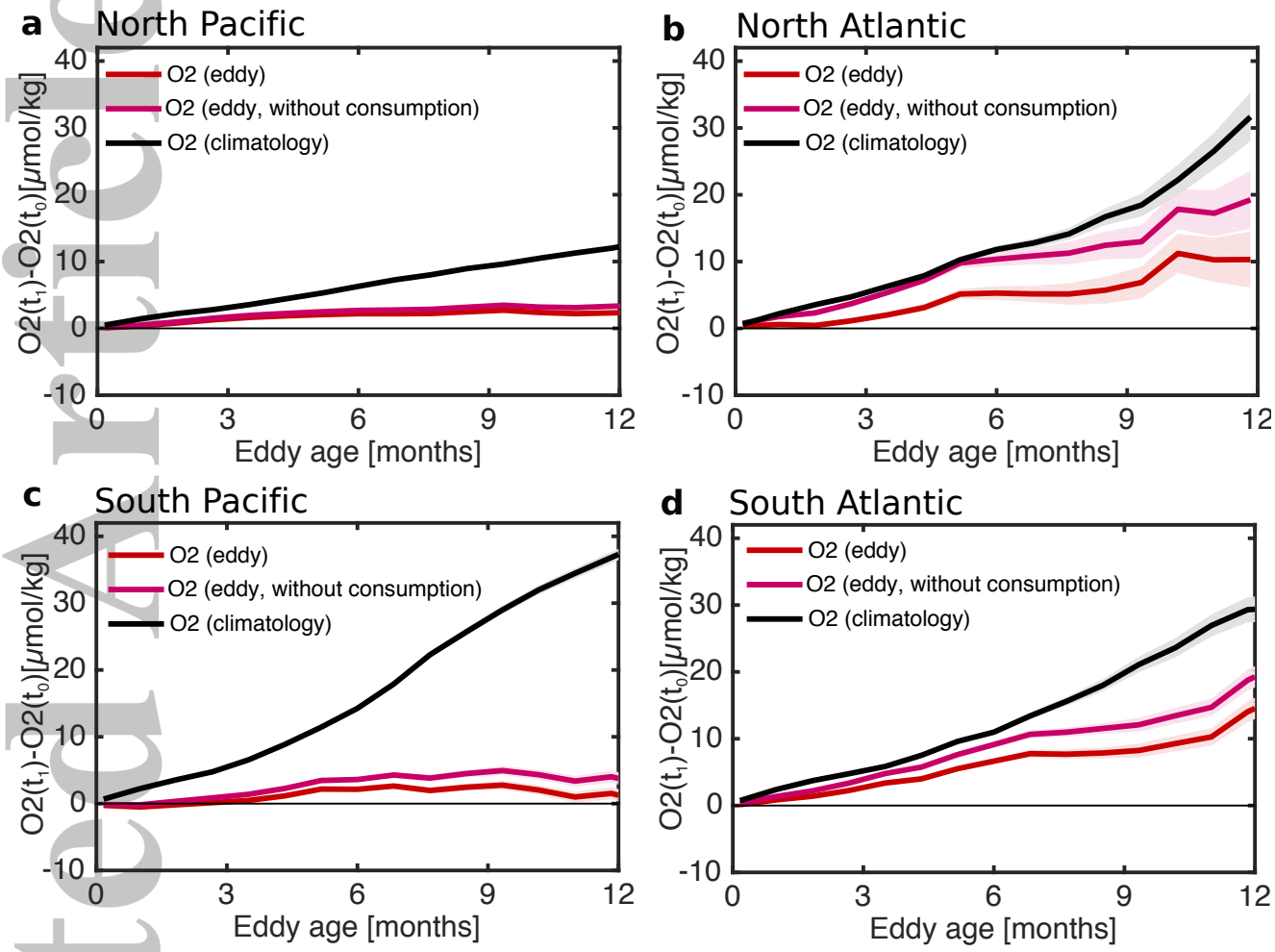

Figure 11. Temporal evolution of oxygen in Puddies existing 3 months or longer. Red lines show oxygen (O2) at eddy centers on the isopycnal layer 26.7 µmol kg^{-1}, relative to the oxygen at the time of first detection, i.e. eddy origin (1 month bins). Pink lines show the same as red lines, with the accumulated respiration of oxygen within the eddy due to its isolation subtracted, i.e. the pink lines are an estimate of oxygen concentrations if there was no consumption of oxygen. Black lines show climatological oxygen concentrations at the locations where eddies occur relative to oxygen concentrations where the eddies originate from, illustrating changing ambient oxygen concentrations while Puddies propagate westward. Shadings indicate the standard error. Oxygen anomalies are shown in the (a) North Pacific, (b) North Atlantic, (c) South Pacific and (d) South Atlantic, for the first year of eddies propagating westward and originating in climatological oxygen conditions lower than 200 µmol kg^{-1}.

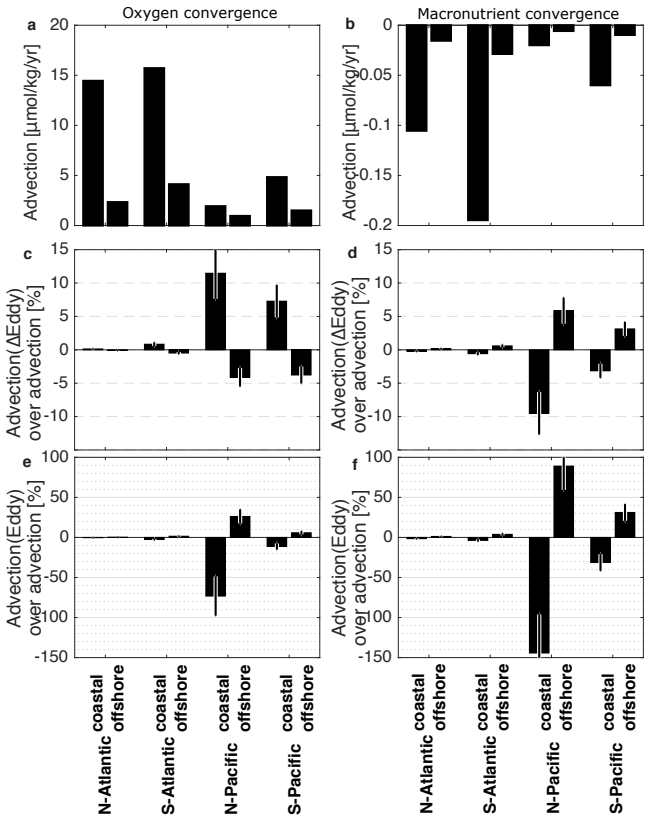

Figure 12. Biogeochemical tracer transport by Puddies. (a,b) Total tracer convergence from resolved advection, which includes transport by Puddies. (c,d) Tracer convergence due to the anomaly transport by Puddies (i.e. advection due to the tracer anomaly ΔC_e inside the eddies, ΔD_e, equation (2a), relative to the advective convergence shown in a,b in %). (e,f) Tracer convergence due to the absolute transport by Puddies (i.e. advection due to the tracer content C_e of eddies, D_e, , equation (2), relative to the advective convergence shown in a,b in %). Panels (a,c,e) refer to oxygen and (b,d,f) to the macronutrient; error bars in (c-f) indicate uncertainty due to eddy radii, thickness and numbers (see Methods section 2.4.1); only eddies existing 9 months or more which tend to propagate $\mathcal{O}$(1000 km) are considered.